Pharmacological Research 210 (2024) 107491

Contents lists available at ScienceDirect

Pharmacological Research

journal homepage: www.elsevier.com/locate/yphrs

Nanoparticles encapsulating phosphatidylinositol derivatives promote neuroprotection and functional improvement in preclinical models of ALS *via* a long-lasting activation of TRPML1 lysosomal channel

Valentina Tedeschi [a,1], Valeria Nele [b,1], Valeria Valsecchi [a], Serenella Anzilotti [c], Antonio Vinciguerra [d], Laura Zuccaro [e,f], Maria Josè Sisalli [g], Chiara Cassiano [b], Nunzia De Iesu [h], Giuseppe Pignataro [a], Lorella Maria Teresa Canzoniero [c], Anna Pannaccione [a], Giuseppe De Rosa [b,*], Agnese Secondo [d,*]

[a] *Division of Pharmacology, Department of Neuroscience, Reproductive and Odontostomatological Sciences, School of Medicine, University of Naples "Federico II", Via S. Pansini 5, Naples 80131, Italy*
[b] *Department of Pharmacy, University of Naples "Federico II", Via D. Montesano 49, Naples 80131, Italy*
[c] *Department of Science and Technology-DST, University of Sannio, Via Port'Arsa 11, Benevento 82100, Italy*
[d] *Department of Biomedical Sciences and Public Health, School of Medicine, University "Politecnica Delle Marche", Via Tronto 10/A, Ancona 60126, Italy*
[e] *Biogem Scarl, Istituto di Ricerche Genetiche, Ariano Irpino, AV, Italy*
[f] *Department of Translational Medical Sciences, Università degli Studi della Campania "Luigi Vanvitelli", Naples, Italy*
[g] *Department of Translational Medical Sciences, University of Naples "Federico II", Via S. Pansini 5, Naples 80131, Italy*
[h] *IRCCS SYNLAB SDN S.p.A., Naples 80143, Italy*

A R T I C L E I N F O

Keywords:
SANP
Neuroprotection
Autophagy
TRPML1
PI(3,5)P2
ALS

A B S T R A C T

Amyotrophic lateral sclerosis (ALS) is a progressive neurodegenerative disease currently incurable, in which motor neuron degeneration leads to voluntary skeletal muscle atrophy. Molecularly, ALS is characterized by protein aggregation, synaptic and organellar dysfunction, and Ca^{2+} dyshomeostasis. Of interest, autophagy dysfunction is emerging as one of the main putative targets of ALS therapy. A tune regulation of this cleansing process is affordable by a proper stimulation of TRPML1, one of the main lysosomal channels. However, TRPML1 activation by $PI(3,5)P_2$ has low open probability to remain in an active conformation. To overcome this drawback we developed a lipid-based formulation of $PI(3,5)P_2$ whose putative therapeutic potential has been tested in *in vitro* and *in vivo* ALS models.

Pharmacodynamic properties of $PI(3,5)P_2$ lipid-based formulations (F1 and F2) on TRPML1 activity have been characterized by means of patch-clamp electrophysiology and Fura-2AM video-imaging in motor neuronal cells. Once selected for the ability to stabilize TRPML1 activity, the most effective preparation F1 was studied *in vivo* to measure neuromuscular function and survival of $SOD1^{G93A}$ ALS mice, thereby establishing its therapeutic profile.

F1, but not $PI(3,5)P_2$ alone, stabilized the open state of the lysosomal channel TRPML1 and increased the persistence of intracellular calcium concentration ($[Ca^{2+}]_i$). Then, F1 was effective in delaying motor neuron loss, improving innervated endplants and muscle performance in $SOD1^{G93A}$ mice, extending overall lifespan by an average of 10 days. Of note F1 prevented gliosis and autophagy dysfunction in ALS mice by restoring $PI(3,5)P_2$ level.

Our novel self-assembling lipidic formulation for $PI(3,5)P_2$ delivery exerts a neuroprotective effect in preclinical models of ALS mainly regulating dysfunctional autophagy through TRPML1 activity stabilization.

* Corresponding authors.
E-mail addresses: gderosa@unina.it (G. De Rosa), a.secondo@staff.univpm.it (A. Secondo).
[1] Equal contribution

https://doi.org/10.1016/j.phrs.2024.107491
Received 12 July 2024; Received in revised form 28 October 2024; Accepted 31 October 2024
Available online 2 November 2024

1. Introduction

Amyotrophic lateral sclerosis (ALS) was firstly described by Charcot and Joffroy in the late 19th century, but, in consideration of the very limited spectrum of curative therapies, it is still regarded as an urgent medical need. ALS is a devastating disease having an unfavourable prognosis due to the progressive degeneration of motor neurons in spinal cord and cortex that, in turn, may lead to a rapid neuromuscular denervation and atrophy of voluntary skeletal muscles [1]. In most of cases, ALS may rapidly conduct patients to paralysis and death in 2–3 years. Several pathomechanisms have been identified [2]. For instance, ubiquitin-positive inclusions of mutant SOD1, TDP-43, FUS, and C9orf72 have been reported in familial ALS, while abnormal aggregation of their wild-type forms is also widely diffused in the brain of sporadic ALS patients [3–6]. Therefore, a significant impairment of proteome degradative mechanisms or protein quality control leads to the aberrant accumulation of aggregated misfolded proteins. As a consequence, many cellular mechanisms become dysregulated in ALS motor neurons, determining synaptic dysfunction, altered ionic homeostasis and excitability, endoplasmic reticulum (ER) stress, mitochondrial dysfunction etc. [7]. Of note, disturbances in Ca^{2+} homeostasis have been considered a pivotal factor determining motor neuronal degeneration in ALS [8]. An interesting aspect is the emerging role of lysosomal Ca^{2+} homeostasis as putative targeting mechanism. Of note, in mice carrying mutations in FIG4, a component of the enzymatic complex regulating the activity of lysosomal channels and ionic homeostasis, autophagy intermediates accumulate in the spinal cord and produce brain lethality [9]. In fact, a severe neurodegeneration occurs with significant loss of neurons and precocious lethality in these mice [9]. To date, genetic deleterious mutations of FIG4 have been considered as a causal gene of familial and non-familial ALS accounting for about 3 % of all ALS cases [10,11].

Despite the increasing knowledge on ALS pathomechanisms, effective medications are still lacking. Recently, the improvement of lysosomal function through the stimulation of the transient receptor potential channel mucolipin 1 (TRPML1; also known as MCOLN1) has emerged as a promising strategy against neurodegeneration occurring in ALS and other neurodegenerative diseases [12]. TRPML1 is a non-selective cation channel expressed on endo-lysosomal vesicles regulating a plethora of lysosomal functions including autophagy. In fact, this cleansing mechanism of defective organelles and misfolded proteins can act through the degradative action of autolysosome, being under the control of lysosomal function itself. Therefore, dysfunction of lysosome may variously affect autophagy.

Under physiological conditions, Ca^{2+} release by TRPML1 is able to trigger a transductional cascade of events leading to the activation of Transcription factor EB (TFEB), the master regulator of autophagy [13]. Molecularly, Ca^{2+} released from TRPML1 induces the activation of the calmodulin-dependent serine/threonine phosphatase calcineurin, that, in turn, triggers TFEB nuclear translocation upon dephosphorylation. This can increase the autophagic flux by promoting lysosomal biogenesis and preparing the machinery deputed to efficiently degrade dysfunctional organelles and aggregates [14,15].

Previous evidence showed a neuroprotective effect of TRPML1 stimulation by ML-SA1 in an *in vitro* neurotoxic model of ALS [16]. The molecular mechanism underlying this neuroprotection consisted in the restoration of organellar Ca^{2+} dyshomeostasis in consideration of the strict relationship between lysosomes and endoplasmic reticulum, thereby counteracting ER stress dysfunction [16]. Moreover, the initial lysosomal Ca^{2+} release upon TRPML1 stimulation can promote a reactivation of the autophagic flux, thus inducing neuroprotection in a preclinical model of ALS. Furthermore, dysfunctional lysosomal Ca^{2+} homeostasis and lysosomal function could be rescued by TRPML1 pharmacological activation in fibroblasts from FIG4-related ALS patients [17]. Therefore, boosting the efficiency of autophagy can protect against toxic aggregates in ALS [18].

From a therapeutic point of view, the imbalance of proteome homeostasis and autophagy opened wide important routes for the identification of more effective therapeutical approaches in ALS [19]. For instance, boosting the clearing mechanisms such as autophagy might be considered a novel therapeutic strategy to rescue motor neuron dysfunction in ALS [16,18]. Currently, the efficacy of some molecules and drugs inducing autophagy is being monitored either in preclinical or clinical trials. Among others, rapamycin, inhibiting mTOR and stimulating autophagy through the formation of autophagosomes from the phagophore [20,21], may determine an improvement of memory and a rescue of motor dysfunctions in a TDP-43 mouse model [22]. Therefore, the activation of autophagy is under clinical investigation [23]. However, this newly identified approach suggests the necessity to discover new pharmacological molecules upregulating the clearing process in ALS. On the other hand, a coarse enhancement of autophagy seems to exacerbate axonal degeneration of ALS motor neurons [24,25] highlighting the precaution of a finest pharmacological strategy.

In consideration of the interest to invest on TRPML1 pharmacological modulation, it could be important to start from the evidence that, showing a greater stabilization of the open state of this lysosomal channel, ML-SA1 synthetic agonist can use distinct activation sites on TRPML1 than that bound by the endogenous ligand $PI(3,5)P_2$ (phosphatidylinositol 3,5-bisphosphate) [26]. However, the use of an endogenous ligand or its chemical modification is an attractive perspective in pharmacotherapy. In this case, a putative neuroprotective action could require a stable and long-lasting effect on the lysosomal channel, which in turn will demand an efficient intracellular and lysosomal delivery of the active component. With this in mind, we investigated the use of $PI(3,5)P_2$, in free form or encapsulated in self-assembling lipid nanoparticles (SANPs). These formulations offer several advantages, including remarkable biocompatibility, high payload encapsulation efficiency and intracellular release, and a straightforward assembly approach based on component mixing. Furthermore, this approach allows the easy integration of further components in the preparation protocol [27]. In detail, SANPs are composed of a calcium phosphate core enveloped by a lipidic coating with a tuneable lipid composition, that have been successfully used for the delivery of anionic chemical entities, e.g. bisphosphonates, siRNAs and miRNAs, especially for applications on central nervous system (CNS) diseases [28–31].

Therefore, SANPs containing $PI(3,5)P_2$ have been prepared and characterized *in vitro* to establish their biophysical and pharmacodynamic properties in modulating TRPML1 and *in vivo* to study their ability in reestablishing autophagic flux and survival. To this aim, lipid SANP formulation containing $PI(3,5)P_2$ was *icv* administered to $SOD1^{G93A}$ mice, a very useful transgenic model of ALS. Here, we show that SANP formulation F1 -containing $PI(3,5)P_2$ - stabilized TRPML1 in an active state moving Ca^{2+} and, when administered *icv* at disease onset, improved muscle performance and extended survival of $SOD1^{G93A}$ mice by reducing gliosis and regulating autophagy.

2. Material and methods

2.1. Synthesis of self-assembling nanoparticles (SANPs)

2.1.1. Materials

N-palmitoyl-sphingosine-1-{succinyl[methoxy(polyethylene glycol) 2000]} (Cer_{16}-PEG_{2000}), 1,2-distearoyl-sn-glycero-3-phosphoethanolamine-N-[methoxy(polyethylene glycol)-2000] (ammonium salt) ($DSPE\text{-}PEG_{2000}$), and 1,2-dioleoyl-3-trimethylammonium-propane (chloride salt) (DOTAP) were purchased from Avanti Polar Lipids (Alabaster, USA). Calcium chloride ($CaCl_2$), sodium phosphate dibasic (Na_2HPO_4), sodium hydroxide (NaOH), and Amicon Ultra-0.5 Centrifugal Filter 30 kDa MWCO were purchased from Merck Life Science S.r.l. (Milano, Italy). Phosphatidylinositol 3,5-bisphosphate diC8 ($PI(3,5)P_2$ diC8-PIP) was purchased from Tebu-Bio (Magenta (MI), Italy). Solvents

Table 1
Composition of the SANP formulations used in this study.

SANP Formulation	Lipid composition	$[PIP]_{SANP}$
F1 SANP PIP (F1)	DOTAP:Cer_{16}-PEG_{2000}	0.33 mg/ML
F2 SANP PIP (F2)	DOTAP: DSPE-PEG_{2000}	0.33 mg/ML
F0' SANP (F0')	DOTAP:Cer_{16}-PEG_{2000}	-
F0'' SANP (F0'')	DOTAP: DSPE-PEG_{2000}	-

for liquid chromatography electrospray ionization tandem mass spectrometric (LC/ESI-MS/MS), namely Water LC-MS Water, LC-MS Ultra CHROMASOLV™ (Honeywell Riedel-de Haën™) and Acetonitrile, LC-MS Ultra CHROMASOLV™ (Honeywell Riedel-de Haën™) were purchased from Exacta+Optech Labcenter S.p.a. (San Prospero (MO), Italy).

2.1.2. CaP NPs synthesis

CaP NPs were prepared by adding an aqueous solution of 10.8 mM Na_2HPO_4 (pH 9.5) to an aqueous solution of 18 mM $CaCl_2$ (pH 9.5) in a 1:1 v/v ratio dropwise while stirring. The CaP NPs suspension was left to stir for 10 min and filtered through 0.22 μm pore-sized polycarbonate filters (MF-Millipore, MicroglassHeim, Italy). The CaP NPs suspension was then stored at 4 °C prior to use.

2.1.3. Liposome preparation

PEGylated liposomes (PLs) were prepared by the thin film hydration method followed by extrusion. Briefly, the lipids in the appropriate ratios were dissolved in a chloroform:methanol mixture (2:1 v/v) and placed in a 50 ML round bottom flask. The organic solvent mixture was removed by rotary evaporation (Laborota 4010 digital, Heidolph, Schwabach, Germany) and the obtained lipid film was hydrated with distilled water for 2 hours at 65 °C. The vesicle suspension was extruded through pore-sized polycarbonate membranes (Nucleopore Track-Etched 25 mm membrane, Whatman, Brentford, UK) by using a thermobarrel extruder (Lipex Extruder, Evonik, Essen, Germany) at 65 °C. More specifically, the vesicle suspension was forced to pass sequentially through 400 nm membranes (3 passages), 200 nm membranes (3 passages), and 100 nm membranes (5 passages). The lipid compositions of the PLs were DOTAP:DSPE-PEG_{2000} (1:0.125 mM) and DOTAP:Cer_{16}-PEG_{2000} (1:0.125 mM).

2.1.4. Self-assembling nanoparticles (SANPs) preparation

In order to form CaP NPs-PIP complexes, 100 μL of an aqueous solution containing PIP at 1 mg/ML were added to 100 μL of CaP NPs; the suspension was vortexed and allowed to react at room temperature for 10 minutes. The CaP NPs-PIP suspension was then added dropwise to 100 μL of PLs; the formulation was vortexed and allowed to react for 25 minutes obtaining PIP-loaded SANPs. The SANP formulations used in this study are reported in Table 1. As a control, SANPs were also prepared in the absence of PIP.

2.1.5. Physico-chemical characterization of PLs and SANPs

PLs, SANPs, and PIP-loaded SANPs were characterized in terms of colloidal dimensions, polydispersity index (PDI), and surface charge by using a Zetasizer Ultra (Malvern, UK). Prior to the measurements, samples were diluted to 1 % in filtered deionized water. For each formulation the z-average diameter, PDI, and zeta potential were calculated as mean ± standard deviation of measurements from three independent batches.

2.1.6. Determination of PIP encapsulation within SANP formulations

In order to determine the extent of PIP loading within SANP formulations, the F1 and F2 formulations were prepared as described above and the concentration of unencapsulated PIP was measured by LC/ESI-MS/MS. Prior to the analysis, the PIP-loaded nanoparticles were separated from the outer medium by using Amicon centrifugal filters (Ultra-0.5 30 kDa MWCO); centrifugation was carried out in a D1524R centrifuge (DLAB SCIENTIFIC CO., LTD., Beijing (China)) at 4000 rcf for 10 minutes. The fluid eluted from the Amicon filters was analyzed with LC/ESI-MS/MS to determine the concentration of unencapsulated PIP. Samples for the standard curve were prepared by diluting a PIP stock solution in water in a dilution buffer to reach the desired concentration. The dilution buffer was obtained by preparing a blank SANP formulation and by separating the nanoparticles from the outer medium with Amicon centrifugal filters (Ultra-0.5 30 kDa MWCO); centrifugation was carried out in a D1524R centrifuge (DLAB SCIENTIFIC CO., LTD., Beijing (China)) at 4000 rcf for 10 minutes. The fluid eluted from the Amicon filters was used as dilution buffer for the standard curve samples.

LC/ESI-MS/MS analysis of PIP was performed using an LTQ-XL mass-spectrometer (Thermo Fisher Scientific) equipped with an H-ESI probe. Mass spectrometer was operated in the negative ion mode employing following source parameter optimized by infusion of PIP standard solution: ion-spray voltage of −2.9 kV, Sheat gas flow rate 35 (Arb), Auxiliary flow rate 5 (Arb), Capillary Temperature 320°C, Heater temperature 150 °C, Capillary Voltage −31.00 Tube Lens −147.54. Two SRM transition have been selected and employed for quantification and confirmation (745.3→647.3 and 372.4→665.3).

Chromatographic separation was performed with an Ultimate 3000 UHPLC (Thermo Fisher Scientific) and employing a Kinetex EVO C18 column, 2.1 × 50 mm, 1.7 μm (Phenomenex, CA). Mobile phase A was Water and mobile phase B was Acetonitrile both containing 0.1 % v/v N, N-Diisopropylethylamine (DiiPEA). Flow rate was set at 0.4 ML/min and column oven was kept at 45° C. Separation was achieved by means of a linear gradient of B from 5 % to 95 % of B in 9 minutes. The column was washed and re-equilibrated for 3 minutes between the injections. A five-points calibration curve (0.078–0.156–0.312–0.625–1.25 ppm) was analyzed in duplicate together with the samples.

2.2. Ex vivo experiments

2.2.1. Human sample collection

All the procedures have been approved by the Ethic and Scientific Committee of "Federico II" University of Naples, School of Medicine (PT 1118/19). Human medulla oblongata tissues from controls (n=3; 2 males and 1 female) and ALS patients (n=6; 2 males and 4 females) were from IDIBAPS Biobanc (Barcelona, Spain). Non-ALS patients with lower scores of dementia have been considered as controls. In these subjects, neuropathologic features have been evaluated by a "ABC" score [32] where "A" represents the deposition of Aβ/amyloid plaques determined by the method of Thal *et al.* [33], "B" represents NFT stage determined by the method of Braak [34,35], while "C" represents neuritic plaque quantified by the method of CERAD [34–36]. Non-ALS patients (controls) have been classified as "A0B1C0". Of note, ALS patients have been classified as pure and sporadic carrying dysfunction of TAR DNA binding protein 43 (TDP-43). TDP-43 is a versatile RNA/DNA binding protein involved in RNA-related metabolism, whose inclusion bodies are widely diffused in the brain and spinal cord of the majority of ALS patients. In particular, pure ALS tissues were from patients carrying TDP-43-dependent genetic pathology, while sporadic ALS tissues were from patients affected by non-genetic TDP-43-dependent pathology.

2.3. Preclinical in vitro and in vivo experiments

2.3.1. Cell cultures and treatments

NSC-34 motor neurons displayed a multipolar neuron-like phenotype and expressed either biochemical or functional markers of primary motor neurons [37]. Therefore, this is a widely used model to investigate ALS pathomechanisms and to identify new treatments [38].

NSC-34 motor neurons were grown in Dulbecco's Modified Eagles Medium with 4.5 g/L glucose, 10 % fetal bovine serum (FBS), 2 mM L-glutamine, 100 IU/ML penicillin and 100 μg/ML streptomycin. Cells were plated in Petri dishes or in multiple well cluster plates and kept in a 5 % CO_2 and 95 % air atmosphere at 37°C as previously described [16,

Table 2
List of primary antibodies used in this study.

Antibody	Supplier	Catalog number	Species	Type	Application	Dilution	Tested in
anti-β-actin-peroxidase	Sigma-Aldrich (Milan, Italy)	A3854 (RRID: AB_262011)	Mouse	Monoclonal	WB	1:10000	Tedeschi et al., FASEB J, 2021; Tedeschi et al., Neurobiol Dis, 2023
anti-phospho-AMPKα (Thr172)	Cell Signaling Technology Inc. (Danvers, MA, USA)	2531 (RRID:AB_330330)	Rabbit	Polyclonal	WB	1:1000	Tedeschi et al., Sci Rep, 2019; Sapienza et al., Int J Mol Sci, 2022
anti-ERK2	Santa Cruz Biotechnology Inc. (Dallas, TX, USA)	sc−271458 (RRID: AB_10650127)	Mouse	Monoclonal	WB	1:1000	Martin et al., Front Endocrinol, 2016
anti-GFAP	abcam (Cambridge, UK)	ab7260 (RRID:AB_305808)	Rabbit	Polyclonal	IHC	1:1000	Anzilotti S. et al., Neurobiol Dis, 2021
anti-histone H3	Thermo Fisher Scientific (Waltham, MA, USA)	PA5–16183 (RRID:AB_10985434)	Rabbit	Polyclonal	WB	1:2000	White C.W., Proc Natl Acad Sci U S A, 2020
anti-IBA1	FUJIFILM Wako Pure Chemical Corporation (Osaka, Japan)	019–19741 (RRID: AB_839504)	Rabbit	Polyclonal	IHC	1:1000	Anzilotti S. et al., Neurobiol Dis, 2021
anti-LAMP1	Merck Millipore (Darmstadt, Germany)	AB2971 (RRID:AB_11212777)	Rabbit	Polyclonal	WB	1:1000	Tedeschi et al., Sci Rep, 2019; Tedeschi et al., Neurobiol Dis, 2023
anti-LAMP2	Sigma-Aldrich (Milan, Italy)	L0668 (RRID: AB_477154)	Rabbit	Polyclonal	WB	1:1000	Tedeschi et al., Sci Rep, 2019; Tedeschi et al., FASEB J, 2021
anti-LC3B	GeneTex Inc. (Irvine, CA, USA)	GTX127375 (RRID:AB_11176277)	Rabbit	Polyclonal	WB	1:1000	Tedeschi et al., Sci Rep, 2019; Sapienza et al., Int J Mol Sci, 2022; Tedeschi et al., Neurobiol Dis, 2023
anti-p62/SQSTM1	Novus Biologicals (Littleton, CO, USA)	NBP1–48320 (RRID:AB_10011069)	Rabbit	Polyclonal	WB	1:1000	Tedeschi et al., Sci Rep, 2019; Sapienza et al., Int J Mol Sci, 2022; Tedeschi et al., Neurobiol Dis, 2023
anti-PI(3,5)P_2	Echelon Biosciences Inc. (Salt Lake City, UT, USA)	Z-P035 (RRID: AB_427224)	Mouse	Monoclonal	ICC and IHC	1:1000	Hamel Y., Cell Rep Med, 2021
anti-SMI 32	Covance (Princeton, NJ, USA)	SMI−32R−100 (RRID:AB_509997)	Mouse	Monoclonal	WB	1:1000	López-Erauskin J., Neuron, 2018
anti-TDP43	GeneTex Inc. (Irvine, CA, USA)	GTX114210 (RRID: AB_2038095)	Rabbit	Polyclonal	WB	1:1000	Huang C.C. et al. J Cell Sci, 2014
anti-TFEB	GeneTex Inc. (Irvine, CA, USA)	GTX33541 (RRID:AB_2887718)	Rabbit	Polyclonal	WB	1:1000	Bisicchia E. et al., Cell Death Dis, 2022
anti-TRPML1	Alomone Labs (Jerusalem, Israel)	ACC−081 (RRID:AB_10915894)	Rabbit	Polyclonal	WB	1:1000	Tedeschi et al., Sci Rep, 2019; Tedeschi et al., FASEB J, 2021; Sapienza et al., Int J Mol Sci, 2022
anti-α-tubulin	Sigma-Aldrich (Milan, Italy)	T5168 (RRID: AB_477579)	Mouse	Monoclonal	WB	1:5000	Secondo et al., Stroke, 2019; Tedeschi et al., FASEB J, 2021
anti-phospho-ULK (Ser317)	MyBioSource Inc. (San Diego, CA, USA)	MBS9600629 (RRID: not available)	Rabbit	Polyclonal	WB	1:1000	–

37]. Cells were differentiated with 10 μM retinoic acid and then cultured in fresh medium containing the cyanobacterial β-N-methylamino-L-alanine (L-BMAA) (300 μM/48 h), a neurotoxin described as a low-potency excitotoxin increasing the incidence of ALS and Parkinsonism-dementia complex (PDC) [16,37]. Under these conditions, L-BMAA promotes oxidative and endoplasmic reticulum (ER) stress [37], and it is able to impair the autophagic flux in motor neurons [16]. For electrophysiological and Ca^{2+} imaging experiments, PI(3,5)P_2 has been used as diC8-PI(3,5)P_2, a lipophilic form of this phosphoinositide.

TRPML1 knocking-down was achieved by the following FlexiTube siRNA (Qiagen, Milan, Italy) (10 nM) sense strand: 5′-CAAGAACCUCACACUGAAATT-3′; antisense strand: 5′-UUUCAGUGUGAGGUUCUUGTA-3′ (Mm_Mcoln1_5) [16].

2.3.2. *SOD1^{G93A} ALS mice and treatments*

All the procedures, performed in accordance with European Guidelines for the use of animals in research (2010/63/EU) and the requirements of Italian laws (D.L. 26/2014), were approved by the Animal Care Committee of "Federico II" University of Naples and the Animal welfare office, Department of Public Health and Veterinary, Nutrition and Food Safety, General Management of Animal Care and Veterinary Drugs of the Italian Ministry of Health (589/2020-PR). All efforts were made to minimize animal suffering and to reduce the number of animals.

B6/SJL-Tg(SOD1*G93A)1Gur/J mice were purchased from Jackson Laboratories (Bar Harbor, USA); mice were bred and housed in a virus/antigen-free facility at constant temperature and humidity (between 40 % and 70 %). Then, B6/SJL males harbouring the SOD1^{G93A}

transgene were crossed with wild-type B6/SJL females. Transgenic hemizygous $SOD1^{G93A}$ males were crossbred with C57BL/6 (RRID: MGI:5657312) females and transgenic progeny was genotyped by PCR as previously described [39].

$SOD1^{G93A}$ ALS mice, firstly characterized for testing drugs [40], represent the most commonly used ALS model in international literature. Disease onset was defined at 70 days of age by evaluation of grip strength providing an index of neuromuscular function [41]. To monitor disease progression, behavioural scores and body weight were recorded from at least 49 days of age [42,43]. Disease end stage was defined by full paralysis of hind limbs and loss of the ability to turn within 30 seconds of being positioned on their back. At this stage, mice were sacrificed. In consideration of disease's features, we assigned presymptomatic and late symptomatic terms at 1,5 months and 4,5 months, respectively.

Overall, for behavioural tests 29 male and 42 female mice housed under diurnal lighting conditions (12 h darkness/light) were used; 3 male and 2 female out of these animals were not included in the experimental groups as they died for unknown reasons. Brainstem, spinal cord and cortex tissues from pre-symptomatic 1,5 months-old (n=12) and symptomatic 4,5 months-old (n= 20) $SOD1^{G93A}$ mice were analyzed by Western blotting. In total, n = 108 animals were included in this study. $SOD1^{G93A}$ mice were injected *via icv* with self-assembling nanolipid preparation F1 containing $PI(3,5)P_2$ at 2 different dosages or vehicle solution starting from 1,5 months for the following 6 weeks (1 injection/week).

2.3.3. Electrophysiology of TRPML1-mediated currents

The whole-endolysosome configuration was achieved by a modified patch-clamp method [44–47]. Whole-endolysosome recordings were performed on enlarged vacuoles, obtained treating NSC-34 cells with 1 μM YM201636 for at least 2 hours. The pipette (luminal) solution contained (in mM): 145 NaCl, 5 KCl, 2 $CaCl_2$, 1 $MgCl_2$, 10 HEPES, 10 MES and 10 glucose (pH 4.6 with NaOH), and bath (cytoplasmic) solution contained (in mM): 140 K-Gluconate, 4 NaCl, 1 EGTA, 2 Na2-ATP, 2 $MgCl_2$, 0.39 $CaCl_2$, 0.1 GTP and 10 HEPES (pH 7.2 with KOH and $[Ca^{2+}]_i$ of 100 nM). Cells were held at 0 mV and the currents were elicited by repeated voltage ramps (from −140 to +140 mV; 400 ms) with a 4-s interval between ramps. Bath application of ML-SA1 (10 μM) induced the specific activation of TRPML1-mediated currents (I_{TRPML1}). I_{TRPML1} were recorded using the commercially available amplifier Axopatch 200 B and Digidata 1322 A interface (Molecular Devices). Data were acquired and analyzed using the pClamp software (version 9.0, Molecular Devices). Whole-endolysosome currents were digitized at 10 kHz and filtered at 2 kHz. All experiments were conducted at room temperature (21–23°C) and all recordings were analysed in pCLAMP10 (Molecular Devices).

2.3.4. $[Ca^{2+}]_i$ measurement on single neuron

$[Ca^{2+}]_i$ was detected in motor neuronal cells by single-cell Fura-2/AM computer assisted video-imaging [16]. After loading, cells were alternatively illuminated at wavelengths of 340 and 380 nm and the emitted light was passed through a 512 nm barrier filter. Fura-2/AM fluorescence intensity was measured every 3 s. Results are presented as cytosolic Ca^{2+} concentration calculated by the equation of Grynkiewicz *et al.* [48,49]. Experiments were repeated 3 times on at least 20 cells for each group. SANP-$PI(3,5)P_2$ formulation's activity on $[Ca^{2+}]_i$ was evaluated as Δ% of increase over basal level of calcium and AUC quantified by calculating the integral of $[Ca^{2+}]_i$ responses.

2.4. Nuclear-cytoplasmic fractionation

Cells were lysed in an ice-cold lysis buffer (100 mM NaCl, 50 mM Tris-HCl pH 7.4, 0,2 % SDS, 1 mM EGTA, 1 mM NaF, 1 mM phenylmethylsulfonyl fluoride, 0,5 % NONIDET P-40, 1 mM Na_3VO_4) supplemented with a protease inhibitor mixture (Roche Diagnostics) for 10 min. Then, the lysate was centrifuged for 5 min at 500 g, 4°C. The supernatant represented the cytoplasmic fraction, while pellet was the nuclear fraction. This latter fraction was washed three times, lysed in RIPA buffer and sonicated (2 ×20 seconds). Purity of each fraction was characterized by the expression of specific cytosolic and nuclear markers (i.e. ERK2 and H3, respectively, as reported in Table 2).

2.5. Immunocytochemistry on cell cultures and Western blotting

For immunocytochemistry NSC-34 motor neurons were fixed at room temperature in 4 % paraformaldehyde for 20 min as previously reported [16]. Following several washes in PBS, cells were blocked in 3 % BSA for 30 min and then incubated with one of the specific antibodies reported in Table 2. Finally, cells were also incubated for 5 min with Hoechst. Controls of the method included the replacement of the primary antibody with normal serum. Western blotting experiments were conducted as previously reported [16]. Then, membranes were incubated with the primary antibodies reported in Table 2.

2.6. Cell viability

MTT assay was used to calculate the quantity of cells with active metabolism [50]. Briefly, cells were incubated with 3[4,5-dimethylthiazol-2-yl]-2,5-diphenyl-tetrazolium bromide (0.5 mg/ML in PBS 1 hour/37°C) as reported in Secondo A. *et al.*, Cell Calcium, 2007 [51]. The reduction of tetrazolium salts by dehydrogenases was detected spectrophotometrically at 570 nm. Data are expressed as a percentage of control viability.

3. Animal Tests

3.1. Hindlimb grip test

Mice were housed in standard conditions: constant temperature (22 ± 1°C), humidity (relative, 40 %), a 12-h light/dark cycle and with free access to food and water. ALS mice develop early weakened muscle strength that progressively worsens. Neuromuscular strength and coordination were tested by the hindlimb grip test, a very sensitive way to detect early motor impairment. Each mouse was placed up to a maximum of 100 s on a suspended grid of a conventional housing cage over a soft fall area. The time was recorded from the beginning of the test until the mouse remained griped with at least two limbs. The trial was repeated three times counting the latency for each. The test was stopped if the animal fell more than 10 times. After behavioural tests three/four animals per group were sacrificed for histological analyses.

3.2. Survival rate analysis

Clinical signs of the disease were evaluated daily. Once an animal reached a defined disease endpoint (i.e., when the mouse was unable to stand upright in 30 s once placed on its side), it was euthanized by cervical dislocation. Other euthanasia criteria included a weight loss of more than 20 %, paralysis, hunched posture, and loss of fighting reflexes (from both sides within 15–30 s). Animals with milder motor symptoms that were not able to reach the food grid received food on the ground and water in bottles. Each animal was weighed weekly using a standard scale. Kaplan-Meier survival analysis of death due to the severity of ALS was performed on $SOD1^{G93A}$ mice treated with F1 or vehicle followed until the defined endpoint.

3.3. Tissue processing, immunostaining, and confocal immunofluorescence

Animals were anesthetized and transcardially perfused with saline solution. Then, they were perfused with 4 % paraformaldehyde in 0.1 mol/L PBS saline solution to remove spinal cords that were

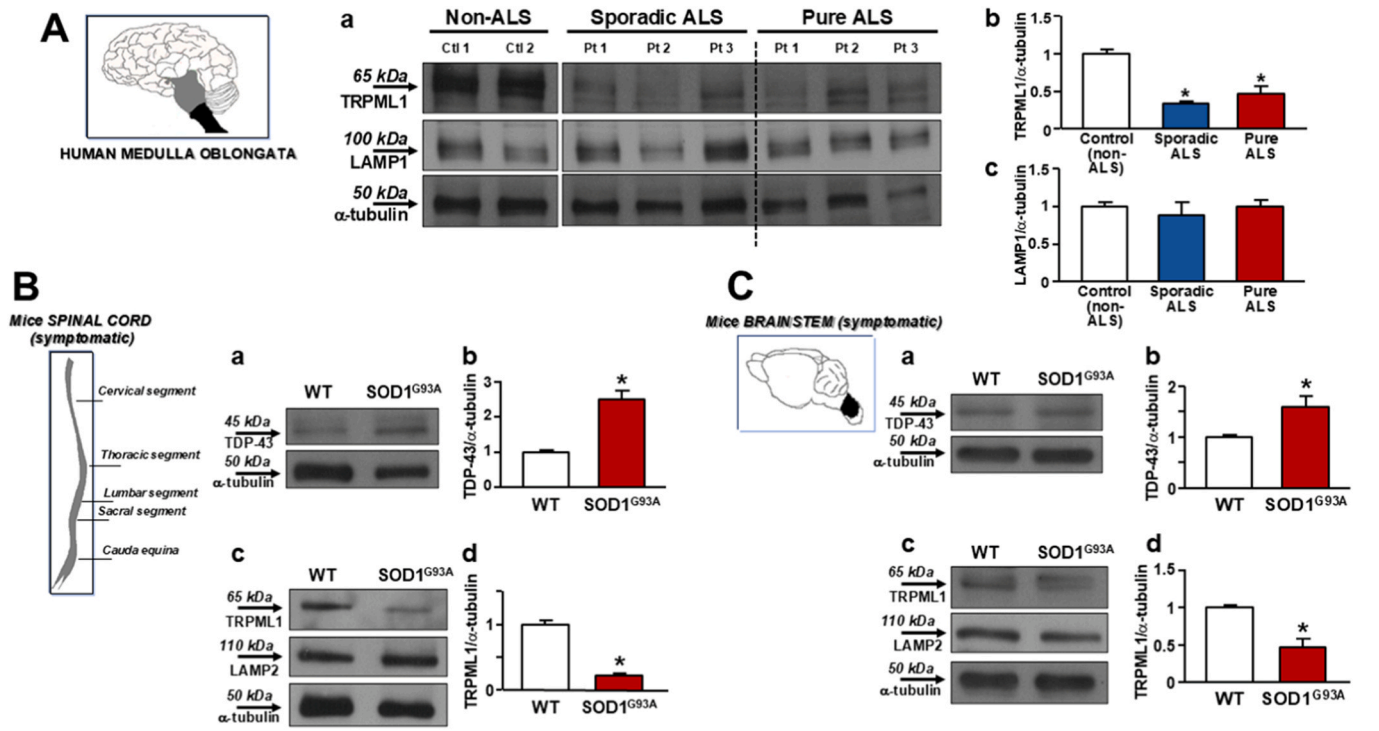

Fig. 1. TRPML1 protein is downregulated in human medulla oblongata *post-mortem* tissues and in the brain of SOD1^{G93A} mice at symptomatic stage, (**A**) Representative Western blotting (a) and quantification of TRPML1 (b) and of LAMP1 expression (c) in non-ALS (controls), pure and sporadic ALS patients. Values were normalized for α-tubulin. Criteria of ALS patients' classification are reported in Material and Methods. Data are presented as means ± SEM. *p<0.05 vs controls. (B) Representative Western blotting of TDP-43 (a), TRPML1 (c), LAMP2 (c) with the relative quantifications (b;d) in spinal cord tissues of symptomatic SOD1^{G93A} mice at 4,5 months. (C) Representative Western blotting of TDP-43 (a), TRPML1 (c), LAMP2 (c) with the relative quantifications (b;d) in brainstem tissues of symptomatic SOD1^{G93A} mice at 4,5 months. The experiments in B and C were repeated at least three times on different samples. Data are presented as means ± SEM. *p<0.05 vs each respective control (WT).

cryoprotected in 30 % sucrose in 0.1 M phosphate buffer (PB) with sodium azide 0.02 % for 24 h at 4°C as previously described [52]. Next, spinal cords were sectioned frozen on a sliding cryostat at 20 μm thickness, in rostrum-caudal direction. Afterwards, free floating serial sections were incubated with PB Triton X 0.3 % and blocking solution (0.5 % milk, 10 % FBS, 1 % BSA) for 1 h and 30 min. Sections were incubated overnight at +4°C with the following primary antibodies: anti-GFAP (abcam, cat #AB7260), anti-IBA1 (Wako, cat #019–19741), and anti-PI(3,5)P_2 (Echelon Biosciences Inc., cat #Z-P035) and then exposed to the corresponding fluorescent-labelled secondary antibodies, Alexa 488/Alexa 594 conjugated anti-mouse/anti-rabbit IgG. Nuclei were counterstained with Hoechst. Images were observed under the Zeiss LSM700 META/laser scanning confocal microscope (Zeiss, Oberkochen, Germany). Single images were taken with a resolution of 1024×1024. Nissl staining was performed as previously described [53]. Briefly, slide-mounted sections were dipped 7 min in 0.5 % solution of Cresyl Violet in distilled water supplemented with acetic acid (16 N solution, 60 drops/l). Slides were then rinsed in distilled water, dehydrated through graded ethanol baths (95 %, 100 %; 5 min each), dilapidated 8 min in xylene, and coverslipped with Eukitt Mounting Medium [54].

3.4. GFAP/Iba1 analysis

Frozen spinal cords were sectioned on a sliding cryostat at 20 μm. Lumbar spinal cord images from the same areas of each spinal cord region were acquired by confocal microscopy. Quantitative analyses were performed using ImageJ software in the total number of positive signals of GFAP and Iba1 antibody for photographic field (mm^2) [55] in lumbar spinal cord (L1-L6). N = 3 spinal cords and three sections for each experimental group were analyzed.

3.5. Motor neurons counting in WT and SOD1^{G93A} mice

Motor neurons (MNs) were counted in the spinal cord of SOD1^{G93A} mice as previously described [56]. Frozen spinal cords were sectioned on a sliding cryostat at 20 μm in rostrum-caudal direction. Analyses were performed using ImageJ software in Polygonal-shaped neurons larger than 150–200 μm^2 with a well-defined cytoplasm, nucleus, and nucleolus for MNs counting.

3.6. PI(3,5)P_2 content analysis in WT and SOD1^{G93A} mice

Confocal analyses of intracellular PI(3,5)P_2 immunosignal were performed in SOD1^{G93A} mice treated with vehicle or F1 by quantification of its fluorescence intensity on tissue sections at the level of the lumbar spinal cord (L1-L6). Briefly, after the incubation of each section with anti-PI(3,5)P_2 and the corresponding fluorescent-labelled secondary antibody (see previous paragraph "Tissue processing, immunostaining, and confocal immunofluorescence"), digital images were taken with 40X objective; identical laser power settings and exposure times were applied to all the photographs from each experimental set. Images were first thresholded to identify the positive signal in Polygonal-shaped neurons larger than 150–300 μm^2 with a well-defined cytoplasm. Data were obtained in n = 3 mice per treatment group considering 3–4 sections for each animal. Results were expressed as mean ± SEM. Differences were analyzed by one-way ANOVA followed by Tukey's post-hoc analysis.

3.7. Statistical analysis

All the statistics were performed using GraphPad Prism software version 8. The experiments were designed to generate groups of equal

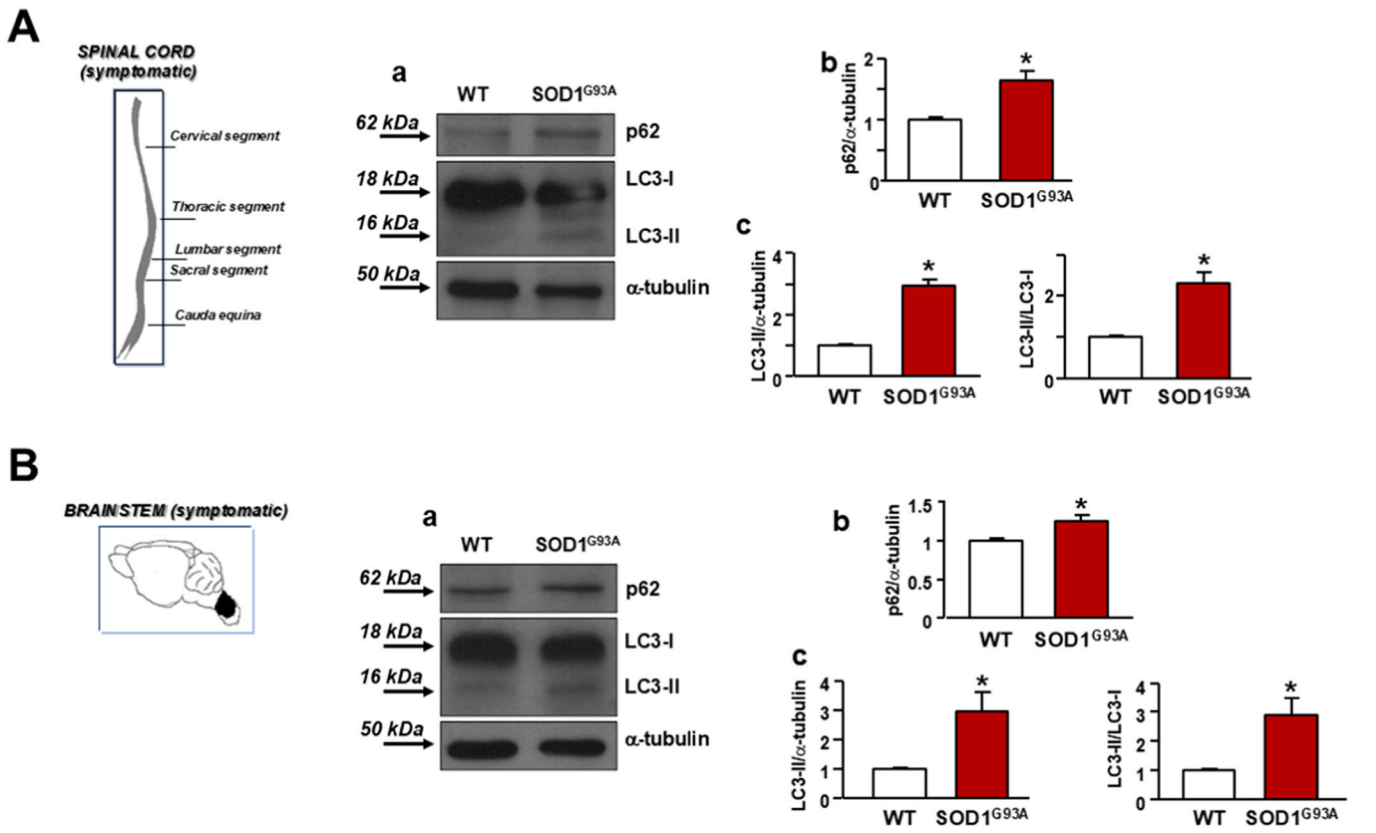

Fig. 2. Autophagy marker expression in the brain of SOD1^{G93A} mice at symptomatic stage, (A) Representative Western blotting of p62, LC3-I and LC3-II (a) with quantifications (b,c) in spinal cord of symptomatic SOD1^{G93A} mice at 4,5 months. Each bar represents the mean ± SEM of data obtained from three different sessions. *p < 0.01 vs each respective control (WT). (B) Representative Western blotting of p62, LC3-I and LC3-II (a) with quantifications (b,c) in brainstem tissues of symptomatic SOD1^{G93A} mice at 4,5 months. Each bar represents the mean ± SEM of data obtained from three different sessions. *p < 0.01 vs each respective control (WT).

size through randomization and blinded analyses. Data are presented as mean ± SEM. Data were analysed using Student's t-test, one-way or two-way ANOVA, as appropriate. Kaplan-Meier Method was used to generate and analyze survival-time data. Post-hoc analyses were carried out using Newman-Keuls, Bonferroni or Tukey tests. The significance level for all the tests was set at 0.05, and a two-tailed p-value < 0.05 was considered statistically significant.

Each group of the *in vivo* tests contained n > 5.

4. Results

4.1. TRPML1 lysosomal channel expression in ALS human tissues and in the brain of ALS mice

Considering the newly identified role of lysosomal dysfunction in the neurodegeneration pathomechanisms [12], lysosomal channels are now described as putative targets in several neurodegenerative diseases [12, 16,57]. In this respect, the non-selective cation channel TRPML1 governs lysosomal homeostasis and function [58]. Of interest, TRPML1 downregulation has been identified as therapeutically solvable, being considered as druggable target in ALS preclinical models [12,16].

In this study, to test the putative dysfunction of TRPML1 expression in ALS patients, medulla oblongata tissues from genetic or sporadic ALS patients carrying TAR DNA binding protein 43 (TDP-43) mutations were analysed. Reduced expression level of TRPML1 protein was detected in medulla oblongata tissues from both genetic and sporadic patients compared with non-ALS patients considered as controls (Fig. 1A a,b). However, the expression of the lysosomal protein LAMP1 remained unchanged in these ALS tissues compared with controls (Fig. 1A a,c).

With the aim to characterize the role of TRPML1 in ALS and identify new pharmacological treatments, the function of this lysosomal channel has been studied in SOD1^{G93A} mice, a widely used animal model of ALS. Symptomatic SOD1^{G93A} mice expressed higher level of TDP-43 protein in spinal cord (Fig. 1B a,b) and brainstem (Fig. 1C a,b) compared with wild-type (WT) mice. Of note, in the same brain areas, they showed significantly reduced protein level of TRPML1 channel (Fig. 1B c,d; 1 C c,d). Moreover, in presymptomatic SOD1^{G93A} mice, TRPML1 protein expression did not change in spinal cord compared with control expression, while it was slightly reduced in brainstem (Supplemental Figure S1).

4.2. TRPML1 protein dysfunction and autophagy in ALS mice

The role of TRPML1 in autophagy regulation has been widely reported [58]. For instance, macroautophagy is reduced in TRPML1-deficient neurons [59], while autophagic flux is significantly enhanced in TRPML1-overexpressing cells [60] as well as in neurons exposed to TRPML1 synthetic agonists [16].

In the light of the previous findings stating the role of autophagy in neurodegeneration [61], autophagy markers were detected in spinal cords and brainstems of ALS mice in order to establish a putative correlation between TRPML1 and resting level of this cleansing process deputed to proteostasis maintenance. Protein expression of the autophagy markers p62 and LC3-II increased in symptomatic SOD1^{G93A} animals compared with WT mice of the same age, thereby confirming the engulfment of this cleansing process in ALS. Specifically, p62 and LC3-II overexpression occurred both in spinal cord (Fig. 2A a-c) and brainstem (Fig. 2B a-c) areas of symptomatic animals. Of note, the same pattern of

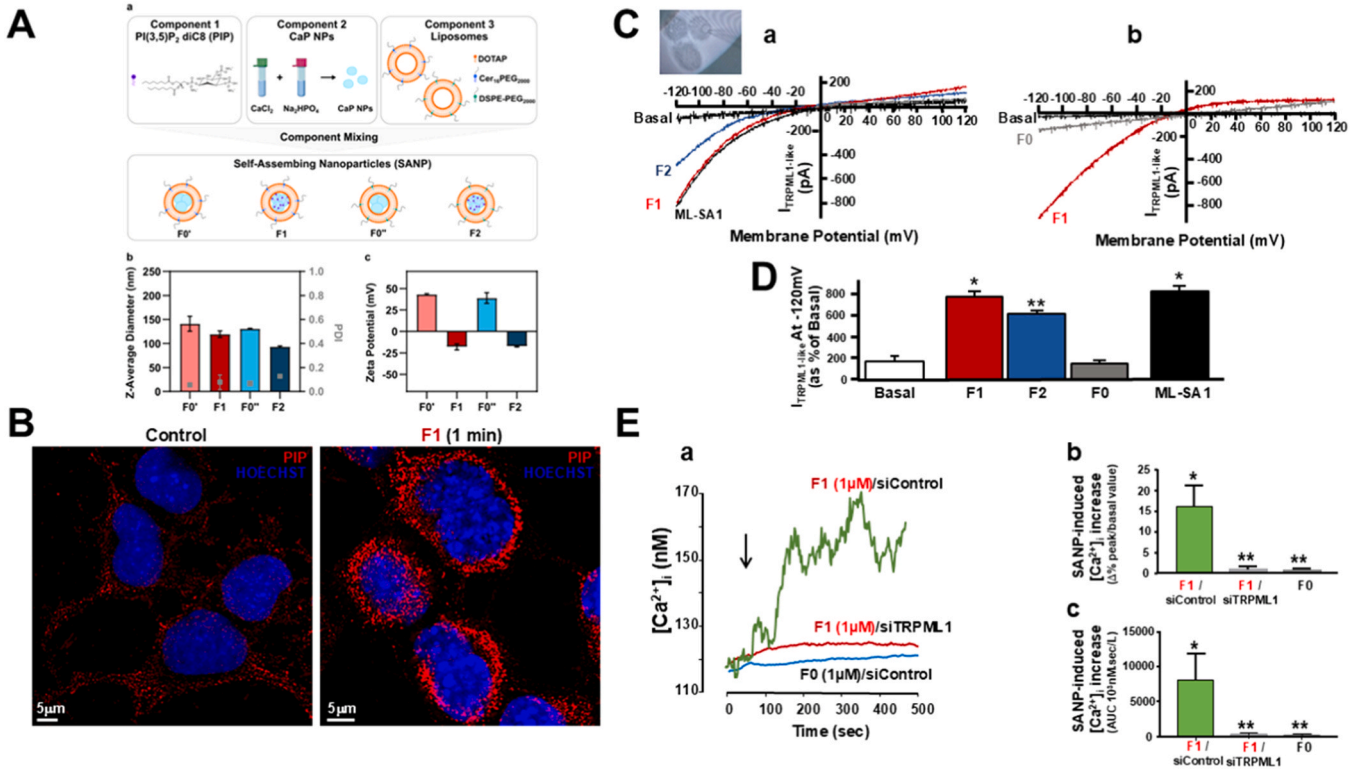

Fig. 3. SANP-PI(3,5)P_2 formulations, F1 and F2, stimulated TRPML1 long-lasting activity detected by patch-clamp and Ca^{2+}-imaging in NSC-34 motor neuronal cells, (A) (a) Schematic representation of SANP-PI(3,5)P_2 preparation (see Material and Methods for more details). Z-average diameter and PDI (b) and zeta potential (c) of SANP formulations prepared in the absence of PIP (F0', F0'') and SANP formulations prepared in the presence of PIP (F1, F2). Data for SANP is reported as mean ± s.d. of n=3 independent batches. **(B)** PI(3,5)P_2 immunosignal in differentiated NSC-34 cells under basal conditions and after **F1** exposure (1 μM/1 min). Scale bars: 5 μm. **(C)** Representative whole lysosome currents in resting conditions and after F1, F2, F0' and ML-SA1 administration (n=5 endolysosomes for each group). F1 and F2 contained equimolar concentration of PI(3,5)P_2. **(D)** Each bar represents the mean ± S.E. of data obtained from three different sessions. *$p < 0.01$ vs basal currents; **$p<0.01$ vs F1-induced currents. (E) (a) Representative traces of $[Ca^{2+}]_i$ measured before and after F1 and F0' administration (at least 30 cells for each group). F1 was added to the cells after transfection with siControl or siRNA against TRPML1. Quantification of "a" as percentage of $[Ca^{2+}]_i$ increase expressed as Δ % (b) and AUCs (c) of $[Ca^{2+}]_i$ responses. Each bar represents the mean ± S.E. of data obtained from three different sessions. *$p < 0.05$ vs each respective basal values; **$p < 0.05$ vs F1.

autophagy markers' expression was detected in both male and female symptomatic ALS animals at the level of brainstem and spinal cord, in which TRPML1 protein was downregulated (Supplemental Figures S2 and S3). Furthermore, symptomatic $SOD1^{G93A}$ mice expressed the same pattern of protein expression (i.e. TDP-43 overexpression, TRPML1 downregulation and p62+LC3-II overexpression) also in cortex (Supplemental Figures S4 and S5), a brain area in which dysfunctional corticomotor neurons play a greater impact on ALS pathological abnormalities [62].

4.3. Effect of different SANP-PI(3,5)P_2 formulations, F1 and F2, on TRPML1 activity detected by patch-clamp and single cell video-imaging in NSC-34 motor neuronal cells

TRPML1 is activated by PI(3,5)P_2, a lysosome-specific phosphoinositide, but not by other lipids [63,64]. Although PI(3,5)P_2 can readily bind and activate TRPML1, the resulting PI(3,5)P_2-bound channel has low open probability and remains mostly in the closed conformation [26]. To enhance the pharmacodynamic properties of PI(3,5)P_2, we developed SANP formulations with varying lipid composition (Table 1); we used a synthetic derivative of PI(3,5)P_2, namely dioctanoyl PI(3,5)P_2 (diC8-PIP), here referred to as PIP. SANP formulations encapsulating PIP were identified as F1 and F2, while SANP formulations prepared in the absence of PIP were named F0' and F0''. SANP had a calcium phosphate (CaP) core enclosed by a lipid shell; the CaP core can complex molecules with a net negative charge (*e.g.*, bisphosphonates and RNA) due to the interaction between calcium ions and the phosphate groups of the payload. Given the presence of phosphate groups in the PIP structure, we hypothesized that SANP could be an ideal platform for its encapsulation and delivery.

PIP-loaded SANP formulations were obtained by mixing PIP, CaP NPs, and cationic liposomes with varying lipid composition (Fig. 3A a). Based on our previous work [30], we chose 1,2-dioleoyl-3-trimethylammoniumpropane (DOTAP) as the cationic lipid and either Cer_{16}-PEG_{2000} or DSPE-PEG_{2000} as the PEGylated lipid. The formulations were characterized in terms of size, polydispersity, and surface charge (Fig. 3A b, c), as well as of PIP encapsulation efficiency. The physico-chemical properties of SANP formulations are reported in Fig. 3A b,c; while the inclusion of PIP did not significantly affect the nanoparticle mean hydrodynamic diameter (Fig. 3A b), a marked reduction in the zeta potential for the PIP-loaded SANP formulations was found (Fig. 3A c). These features suggest that complexation with PIP induced a substantial re-organization of the nanoparticle structure.

To quantify the amount of PIP encapsulated within SANP, we developed a method based on liquid chromatography electrospray ionization tandem mass spectrometry by adapting a previously published protocol [65]. PIP was eluted after 5.2 minutes and we could obtain a linear standard curve (R^2=0.99) in the 0.078–1.25 μg/ML concentration range. The concentration of unencapsulated PIP in SANP was 0014 ± 0003 μg/ML for F1 and 0009 ± 0,0004 μg/ML for F2; since the theoretical PIP concentration in SANP was 330 μg/ML, these data suggest that the encapsulation efficiency of PIP within SANP was approximately 100 %.

Therefore, in the attempt to study the pharmacodynamic properties

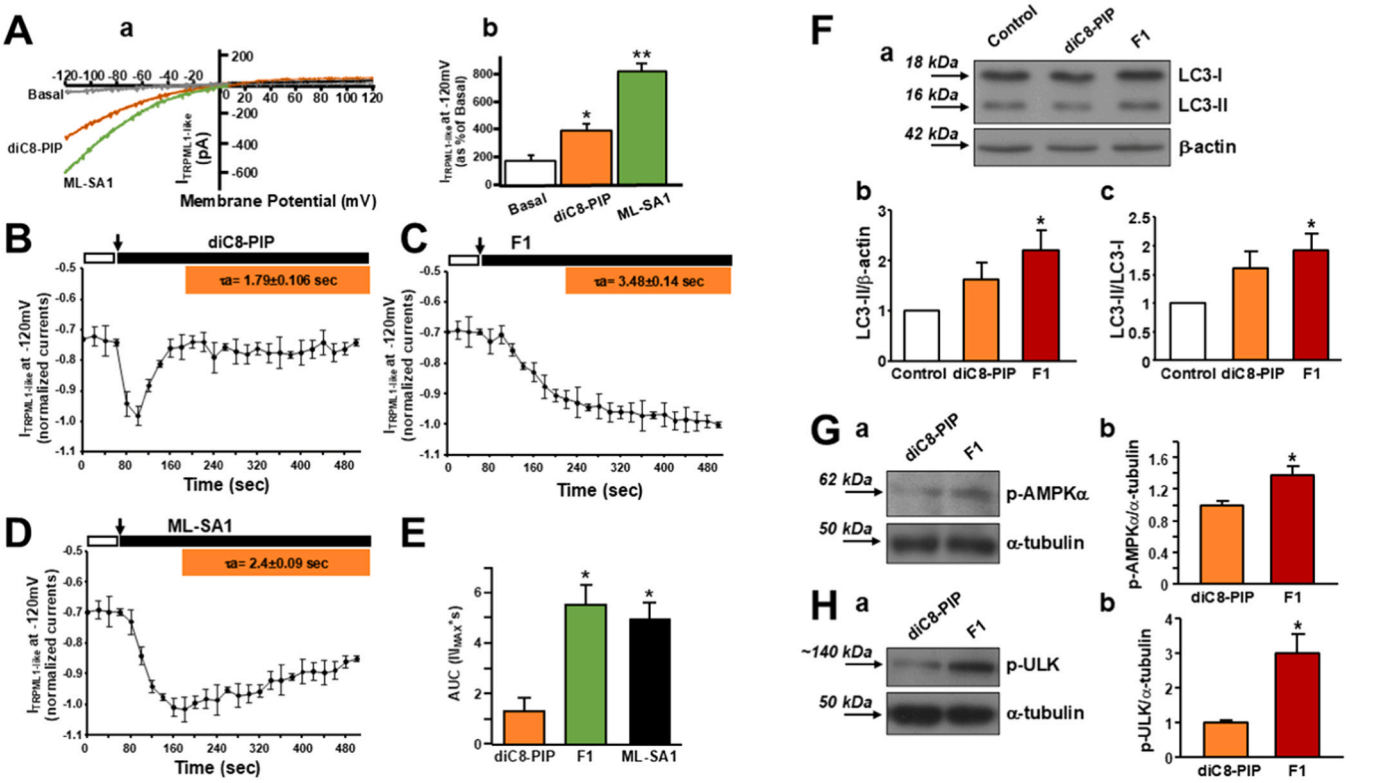

Fig. 4. Biophysical properties of F1- stimulated TRPML1 and autophagy induction in NSC-34 motor neuronal cells, (A) Representative whole lysosome currents (a) and quantification (b) in resting conditions and after administration of ML-SA1 and diC8-PI(3,5)P_2, a lipophilic form of PI(3,5)P_2 (n = 6 endolysosomes for each group). **(B-D)** Representative time-current relationships of TRPML1 activity recorded in the presence of diC8-PI(3,5)P_2 **(B)**, F1 **(C)** and ML-SA1 **(D)**. F1 contains equimolar concentration of diC8-PI(3,5)P_2. **(E)** AUCs of TRPML1 current measured in B-D. Data were obtained from three different sessions. *$p < 0.05$ vs diC8-PI(3,5)P_2. **(F-H)** Representative Western blotting and quantifications of LC3-II **(F)**, p-AMPKα **(G)** and p-ULK **(H)** expression in NSC-34 cells treated with diC8-PI(3,5)P_2 or F1. Data were obtained from 3 different experimental sessions. *$p < 0.05$ vs diC8-PI(3,5)P_2.

of PI(3,5)P_2 formulations, F1 and F2, as well as a SANP formulation lacking the phosphoinositide (namely F0; Fig. 3A), were characterized for their ability to release the phosphoinositide in motor neuronal cells and to modulate TRPML1 biophysics in enlarged endolysosomes. Immunocytochemical experiments revealed that NSC-34 motor neurons expressed basal level of endogenous PI(3,5)P_2 (Fig. 3B, left panel). However, the addition of F1 (1 μM/1 min) significantly enhanced PI(3,5)P_2 immunosignal, displaying a punctuated pattern with perinuclear localization (Fig. 3B, right panel).

Recent development of endolysosome patch-clamp methods has made possible functional study of lysosomal TRPML1 [63,66], a primarily LEL (late endosomes and lysosomes)-localized membrane channel protein [67,68]. Patch-clamp experiments on enlarged lysosomes of NSC-34 motor neuronal cells showed that F1 was more effective than F2 in eliciting a larger inwardly rectifying current encoded by TRPML1 (Fig. 3C-D). Of note, F1 induced a current characterized by the same entity than the synthetic TRPML1 agonist ML-SA1 did (Fig. 3C-D). Moreover, SANP lacking PI(3,5)P_2 failed to modulate basal inwardly rectifying current (Fig. 3C-D).

Being considered a cation channel, lysosomal Ca^{2+} release from TRPML1 was studied after stimulation with F1 in motor neuronal cells loaded with Fura-2/AM (Fig. 3E). Moreover, Ca^{2+} release was measured either as Δ% of basal $[Ca^{2+}]_i$ increase or AUC of the Ca^{2+} responses (Fig. 3E b,c). Of note, F1 promoted lysosomal Ca^{2+} release in NSC-34 motor neuronal cells expressing TRPML1, while it failed to produce the same effect when the channel was silenced with siRNAs (Fig. 3E a-c). F0 formulation, lacking PI(3,5)P_2, failed to induce $[Ca^{2+}]_i$ increase (Fig. 3E a-c), thus showing a specific releasing effect of F1. A further interesting result showed that $[Ca^{2+}]_i$ signal elicited by F1 lasted much more than the rapid signal of the lipophilic form of the pure ligand diC8-PI(3,5)P_2 (data not shown). On the other hand, diC8-PI(3,5)P_2 alone elicited a TRPML1-dependent current amplitude lower than that induced by ML-SA1 administration (Fig. 4A). However, patch-clamp experiments showed that F1 triggered a long-lasting activation of the channel compared with diC8-PI(3,5)P_2 alone, as testified by the significantly longer activation time constant (τa) measured for F1 (**3.48 ±0.14 sec**) compared with that of the pure ligand (**1.79±0.106 sec**) (*$p<0.05$; Fig. 4 B-C). Of note, τa measured for F1-elicited current was similar to that calculated for the synthetic agonist ML-SA1 (Fig. 4D). Furthermore, the AUCs calculated for F1 and ML-SA1 were of the same entity but significantly higher than that calculated for diC8-PI(3,5)P_2 (Fig. 4E).

4.4. Effect of SANP-PI(3,5)P_2 formulation F1 on TRPML1-mediated autophagy in an experimental model of ALS/PDC

It is well established that TRPML1-mediated autophagy is due to the activation of the master regulator TFEB that is constitutively localized in the cytoplasm in an inactive form. Once dephosphorylated by calcineurin -activated by lysosomal Ca^{2+} release- TFEB translocates into the nucleus where it can induce autophagic and lysosomal genes' transcription [13,69]. To test the ability of F1 to promote this cleansing process in response to the biophysical changes of TRPML1 lysosomal channel, the effect on the main initiator of autophagy markers has been tested in NSC-34 motor neuronal cells. Therefore, the efficacy of F1 preparation has been compared with that of the lipophilic derivative of PI(3,5)P_2, diC8-PI(3,5)P_2. Of interest, F1 induced a more rapid and efficient increase in LC3-II, p-AMPKα and p-ULK expression than diC8-PI(3,5)P_2 did (Fig. 4F-H).

Furthermore, TFEB nuclear translocation has been studied in motor

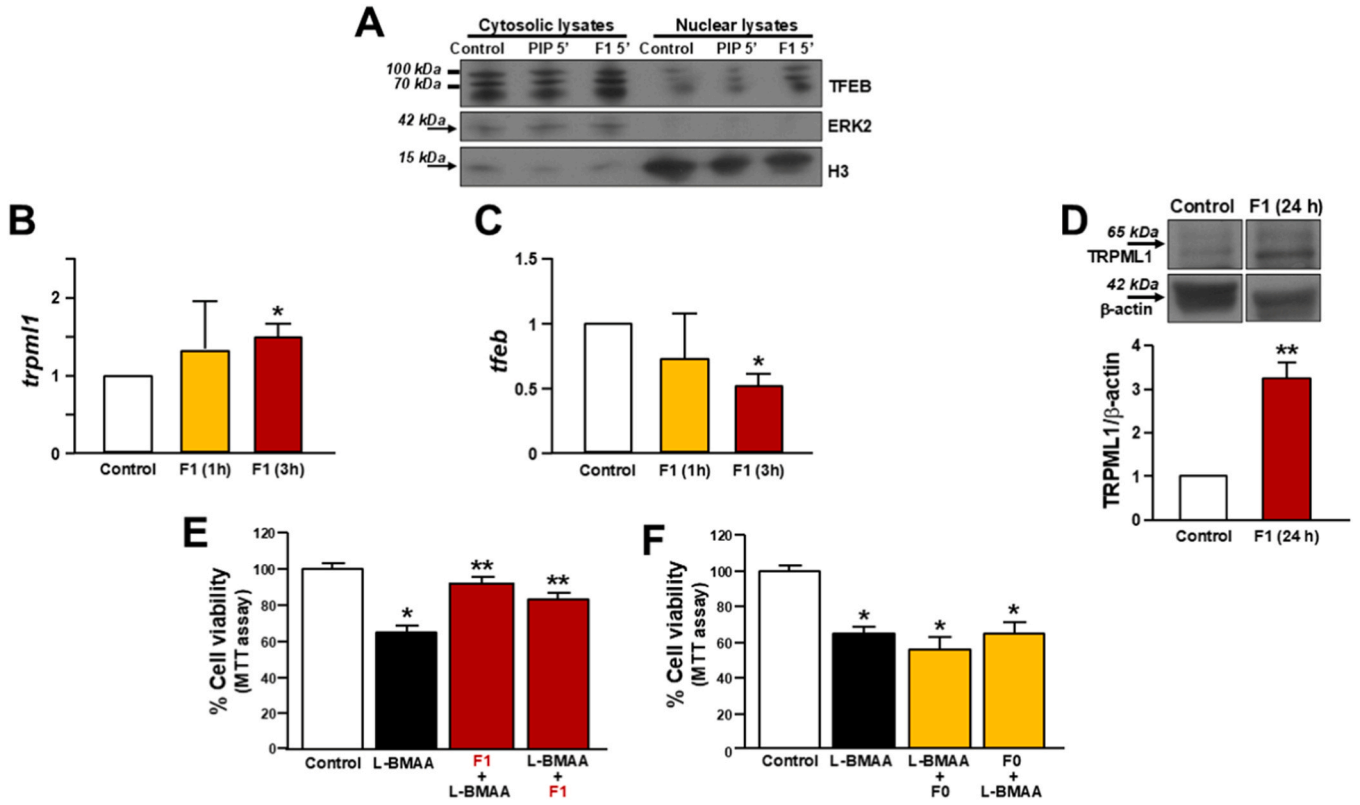

Fig. 5. Downstream effects of F1-induced TFEB nuclear translocation, (A) Representative Western blotting on cytosolic and nuclear extracts from NSC-34 motor neurons exposed to equimolar concentrations of diC8-PI(3,5)P_2 or F1. ERK2 and H3 have been used as housekeeping proteins of cytosol and nuclei, respectively. **(B, C)** qRT-PCR on *trpml1* and *tfeb* expression from NSC-34 samples treated with F1 for 1 and 3 hrs. Each bar represents the mean ± S.E. of data obtained from three different experimental sessions. *$p < 0.05$ vs each control. **(D)** Representative Western blotting and quantification of TRPML1 expression in NSC-34 samples treated with F1 for 24 hrs. Data were obtained from three different experimental sessions. *$p < 0.05$ vs control. **(E,F)** Cell viability of NSC-34 motor neurons exposed to L-BMAA (300 μM/48 hrs) alone and in the presence of F1 or F0'. F1 was preincubated for 5 minutes before L-BMAA or administered after L-BMAA. Each bar represents the mean ± S.E. of data obtained from four different experimental sessions. *$p < 0.05$ vs each control (NSC-34 + vehicle); $^{**}p < 0.05$ vs L-BMAA alone.

neuronal cells exposed to F1 at two different time points. Of note, the master regulator of autophagy was highly expressed in nuclear extracts after 5 minutes (Fig. 5A) but not after 1 hr of exposure (Supplemental Figure S6), thereby demonstrating the timely association with Ca^{2+} release from TRPML1 (Fig. 5A). As a consequence, nuclear translocation of TFEB induced *trpml1* gene transcription as testified by the significant increase in the relative mRNA expression (Fig. 5B). In the meanwhile, this increased expression corresponded to the significant reduction of *tfeb* transcript level (Fig. 5C). Accordingly, TRPML1 protein expression increased thereafter (Fig. 5D).

To test the ability of F1 to interfere with cell suffering in a preclinical model of ALS/PDC, NSC-34 motor neurons were exposed to F1 and F0 at different time points before or after L-BMAA treatment. As previously established, in motor neuronal cells exposed to L-BMAA, mitochondrial activity was significantly reduced as exemplification of general suffering. Preincubation with F1 prevented mitochondrial activity reduction as well as its addition after L-BMAA exposure (Fig. 5E). On the other hand, F0 lacking PI(3,5)P_2 failed to restore mitochondrial activity (Fig. 5F).

4.5. *Effect of SANP-PI(3,5)P_2 formulation F1 on disease progression and SOD1^{G93A} mice survival through autophagy modulation*

Treatment with F1 for six weeks (see protocol reported in Fig. 6) at 10X and 100X during the pre-symptomatic stage prolonged animal survival for approximately 10 days compared with the vehicle group (SOD1^{G93A} Vehicle) (Fig. 6A,B). Furthermore, F1 delayed the evolution of ALS symptoms improving motor function analyzed with grip test performance (Fig. 6C,D). Moreover, the onset of the disease was postponed for approximately 2 weeks (Fig. 6E). F1 treatment attenuated body weight loss in the advanced symptomatic stage of the disease in both male and female mice compared to the vehicle-treated groups (Fig. 6F). Of note, this effect was more prolonged in female animals (Fig. 6F a) than in males (Fig. 6F b).

Moreover, F1 treatment at 10X and 100X reduced the simultaneous overexpression of p62 and LC3-II proteins in the spinal cord of SOD1^{G93A} mice treated for six weeks, thereby counteracting the engulfment of this cleansing mechanism in ALS (Fig. 7A-B). The same result occurred in the brainstem of SOD1^{G93A} mice treated for six weeks with F1 at 10X and 100X (Fig. 7C-D).

ALS motor neuron loss is usually used as a readout of disease progression. In accordance with this evidence, SMI 32 protein expression was highly reduced in the spinal cord of symptomatic SOD1^{G93A} mice treated with the vehicle, but it was restored in F1-treated transgenic mice compared with symptomatic ALS mice (Fig. 8A). The same occurred in the brainstem of symptomatic SOD1^{G93A} treated with F1 (Supplemental Figure S7A-C).

In accordance with the previous evidence, at the end-stage, gallocyanin-based counts of motor neurons showed a significative reduction in symptomatic SOD1^{G93A} mice treated with vehicle (Fig. 8B). Moreover, motor neuron loss was preserved in F1-treated transgenic mice of the same age (Fig. 8B). Of note, F1 treatment reduced astrogliosis and microgliosis -measured as GFAP and IBA1 immunosignals' level- in the ventral horn of SOD1^{G93A} spinal cord compared with transgenic animals exposed to vehicle (Fig. 8C).

Of interest, PI(3,5)P_2 immunosignal was highly reduced in the spinal cord of symptomatic SOD1^{G93A} animals compared with WT mice as sign of impressive reduced level of this phosphoinositide. Moreover PI(3,5)P_2

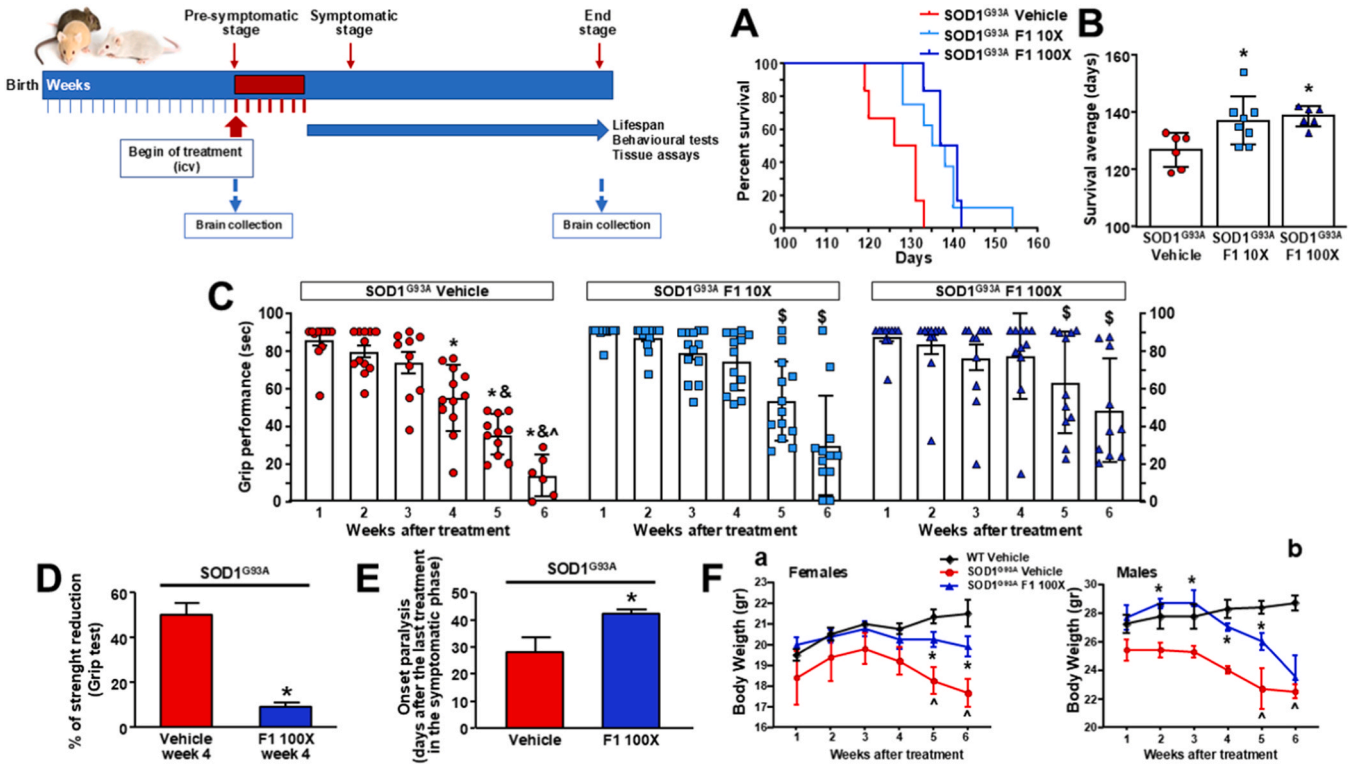

Fig. 6. SANP-PI(3,5)P_2 (F1) treatment from the presymptomatic stage may improve the neuromuscular strength of SOD1^{G93A} mice in the symptomatic stage. On the Top: timeline of experimental design. **(A)** Kaplan-Meier curves showing lifespan of F1-treated SOD1^{G93A} mice intracerebroventricularly injected with the formulation F1 at 10X and 100X/once a week for 6 weeks from the presymptomatic stage (45 days old). The control group consists of SOD1^{G93A} mice injected with physiological solution in the same period of time. **(B)** Quantification of mice lifespan in the three experimental groups. Asterisks (*) indicate a significant difference among F1-treated mice at 10X and 100X and the relative controls (injected with vehicle) calculated by repeated measures two way-ANOVA, $p < 0.05$. (C) Bar graph representing grip performance (in seconds) in relation to the week of treatment. Asterisks (*) indicate a significant difference among the weeks within the group of control ($p<0.05$). $ indicates a significant difference with the same week of control and with previous weeks within the same experimental group ($p<0.05$). (D) Bar graph depicting the neuromuscular strength of SOD1^{G93A} mice treated with F1 100X. Asterisk (*) indicates a significant difference between F1-treated SOD1^{G93A} mice and control group ($p<0.05$). (E) Bar graph depicting the onset of limb paralysis of SOD1^{G93A} mice treated with F1 100X compared to the control group (*$p<0.05$). (F) Line graphs showing body mass evolution of SOD1^{G93A} and wild-type mice (females left panel in a, males right panel in b) injected with physiological solution (SOD1^{G93A} Vehicle and WT Vehicle) or with F1 100X (SOD1^{G93A} F1 100X). Data are presented as means ± SEM. *$p<0.05$ SOD1^{G93A} 100X vs SOD1^{G93A} Vehicle; ^$p<0.05$ vs previous weeks within the same experimental group.

immunosignal was restored in F1-treated transgenic mice (Fig. 9A,B) as a readout of lysosomal function restoration during the treatment.

5. Discussion

The present study builds on the well-documented premise that autophagy, the major degradation pathway of protein aggregates and damaged organelles [70], becomes dysfunctional during ALS progression, fostering the accumulation of detrimental aggregates in suffering motor neurons that project from the spinal cord, brainstem, and motor cortex. Accordingly, many studies on several disease genes strongly suggest that defective mechanisms in different phases of the autophagy pathway are considered as major contributors to ALS pathogenesis. Reinforcing the critical narrative that boosting autophagy is paramount for motor neuron survival [18,71], this study provides concrete evidence on the protective role of lysosomal channels' activation in pushing autophagy in finely and specific way. In particular, the persistent activation of the cationic channel TRPML1 with a lipidic formulation of its endogenous ligand PI(3,5)P_2 may prolong ALS animal survival and reduce motor symptoms by significantly hampering motor neuron loss. This evidence has been raised by an integrated approach based on the synthesis of self-assembling nanoparticles releasing the TRPML1 ligand and preclinical experimentation performed either *in vitro,* with functional techniques on single cell (i.e. patch-clamp and Ca^{2+}-imaging) and biochemical assays on cell cultures (i.e. Western blotting, qRT-PCR, mitochondrial viability), or *in vivo* by using transgenic animals carrying SOD1^{G93A} mutation expressed in ALS patients. The neuroprotective activity of PI(3,5)P_2 formulation has been investigated from a biophysical point of view, showing its stronger ability to activate TRPML1 channel in a more persistent way compared with the free form of the phosphoinositide. This lasting activation may reflect the ability of the new formulation to promote a major channel activation with persistent Ca^{2+} release than the endogenous ligand PI(3,5)P_2 normally still does [64,72]. Consistently, the structure of PI(3,5)P_2-bound TRPML1 seems to remain in a closed conformation [73] thus leading to hypothesize that other endogenous and exogenous factors may participate, cooperatively, in the activation of the lysosomal channel [26]. For instance it has been demonstrated the synergistic activation of TRPML1 by PI(3,5)P_2 and temsirolimus, a rapamycin derivative able to inhibit mTOR-dependent signaling. However, rapamycin and its derivatives may bind also other targets in mTOR-independent way, including TRPML1 [47]. This complex pharmacodynamic activity may further enhance the boosting effect on autophagy thus underlying the neuroprotective profile of temsirolimus in several forms of neurodegeneration [74,75].

The present data clearly identified TRPML1 pharmacological activation as a new putative strategy in ALS therapy. However, several other reports showed the validity of this target modulation in other neurodegenerative diseases characterized by persistent defects of autophagy. An interesting study on Alzheimer's disease (AD) pathomechanisms

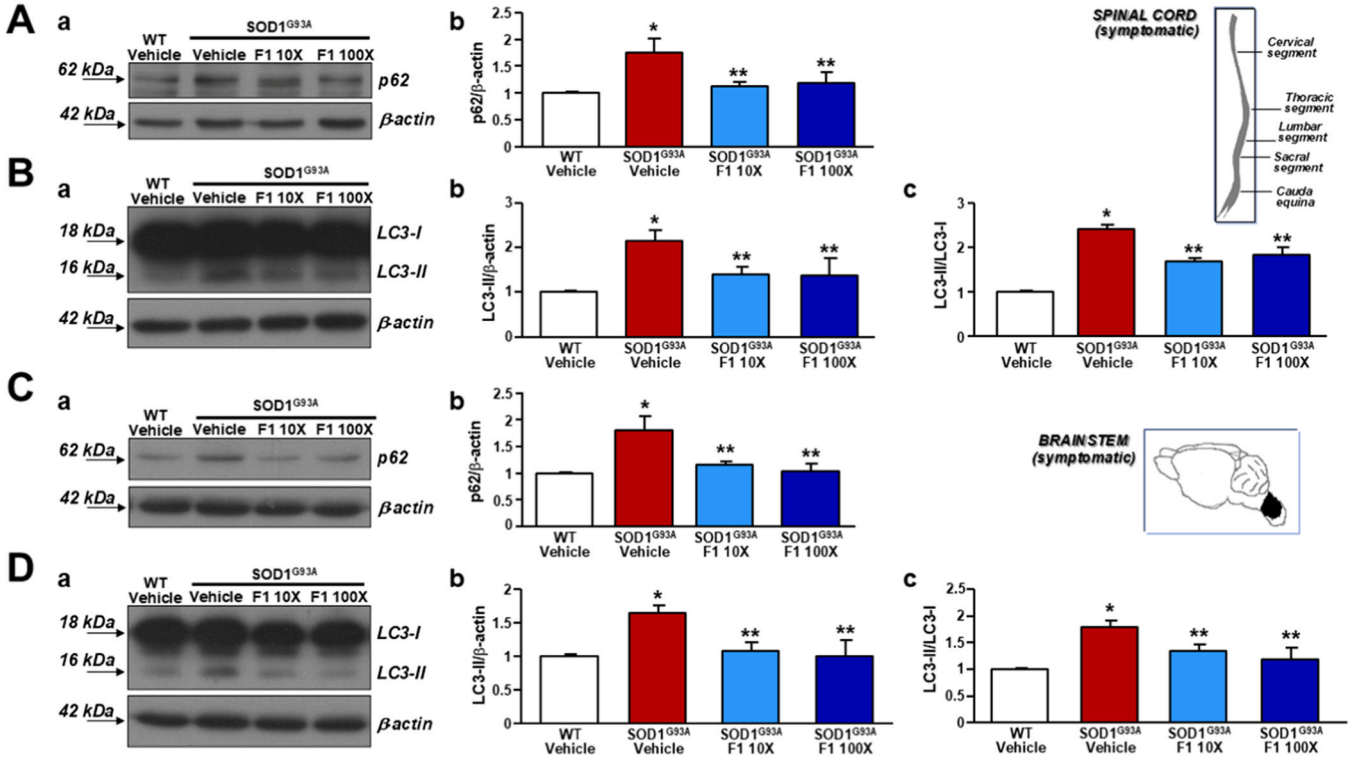

Fig. 7. SANP-PI(3,5)P_2 (F1) treatment from the presymptomatic stage prevented autophagy dysfunction in spinal cords and brainstems of symptomatic SOD1^{G93A} mice at 4,5 months, (**A**) Representative Western blotting (a) and quantification (b) of p62 expression in the spinal cords of WT and SOD1^{G93A} mice injected with physiological solution (WT Vehicle; SOD1^{G93A} Vehicle, respectively), and SOD1^{G93A} mice injected with F1 at 10X and 100X. The last two groups were treated with the preparation once a week for 6 weeks from the presymptomatic stage. Data are presented as means ± SEM. *p<0.05 WT; **p<0.05 vs SOD1^{G93A}. (B) Representative Western blotting (a) and quantification (b) of LC3-II expression in the spinal cords of WT and SOD1^{G93A} mice injected with physiological solution (WT Vehicle; SOD1^{G93A} Vehicle, respectively), and SOD1^{G93A} mice injected with F1 at 10X and 100X. The last two groups were treated as reported in A. Data are presented as means ± SEM. *p<0.05 WT; **p<0.05 vs SOD1^{G93A}. (C) Representative Western blotting (a) and quantification (b) of p62 expression in brainstems of WT and SOD1^{G93A} mice injected with physiological solution (WT Vehicle; SOD1^{G93A} Vehicle, respectively), and SOD1^{G93A} injected with F1 (10X and 100X). The last two groups were treated with the preparation once a week for 6 weeks from the presymptomatic stage. Data are presented as means ± SEM. *p<0.05 WT; **p<0.05 vs SOD1^{G93A}. (D) Representative Western blotting (a) and quantification (b) of LC3-II expression in brainstems of WT and SOD1^{G93A} mice injected with physiological solution (WT Vehicle; SOD1^{G93A} Vehicle, respectively), and SOD1^{G93A} injected with F1 (10X and 100X). The last two groups were treated as reported in A. Data are presented as means ± SEM. *p<0.05 WT; **p<0.05 vs SOD1^{G93A}.

suggests that, in a triple transgenic gp120/APP/PS1 mouse, the functional inhibition of TRPML1 by gp120 facilitates the intraneuronal Aβ accumulation that could be rescued by TRPML1 reactivation [76]. Furthermore, TRPML1 channel expression has been found down-regulated in APP/PS1 transgenic mice while its overexpression can rescue both memory and recognition defects *in vivo*. This neuroprotective action seems to occur, at least partially, through autophagy regulation [77]. Accordingly, AD-like neuronal abnormalities in the endosomal-autophagic-lysosomal defects have been rescued by TRPML1 activation with its synthetic agonist ML-SA1 [78]. More recently, it has been demonstrated that the Chinese medicine compound corynoxine can improve learning and memory function in 5xFAD mice model of AD by increasing neuronal autophagy and lysosomal biogenesis *via* TRPML1/TFEB activation [79]. The same mechanism has been proposed for the therapy of the most common Parkinson's disease (PD). Consistently, ML-SA1 can trigger α-synuclein aggregates' clearance *via* the autophagy-lysosome pathway by TRPML1 activation [80]. Of note, to exert neuroprotection in PD models, TRPML1 can be activated in a direct way or *via* ROS increase by both natural [81] and repurposed drugs [82].

Moreover, in ALS therapy, the present data strongly highlighted the importance of TRPML1 lasting activation in boosting autophagy in order to produce motor neuron survival. In this view, the new lipid-based formulation containing the endogenous activator of TRPML1 should be more effective in boosting autophagy than the endogenous ligand alone, since PI(3,5)P_2 action is characterized by a low channel open probability. Accordingly, the present data showed that the new formulation induced a rapid nuclear translocation of Transcription factor EB (TFEB), the master regulator of autophagy, compared with PI(3,5)P_2 alone. Of note, the time point of TFEB translocation perfectly collimated with that of lysosomal Ca^{2+} release from TRPML1 elicited by this lipid-based formulation in motor neurons, thus demonstrating a strict correlation between the two events. Therefore, the persistent activation of the lysosomal channel may produce the extending effect on ALS mice lifespan and the motor function improvement *via* autophagy restart and/or potentiation. In this context, the reduced expression of the autophagy markers LC3-II and p62 could be interpreted as the physiological recovery of normal autophagy in the dysfunctional brain areas of SOD1^{G93A} mice, mainly affected by the disease. Moreover, an intriguing evidence is that TRPML1 represents not only the promoter of TFEB translocation but also one of its downstream targets [13,83], thus fuelling the maintenance of the autophagic process at neuronal level. In consideration of this evidence, the new formulation may significantly promote the increased expression level of TRPML1 after its stimulation, thus determining a sort of neuroprotective loop that starts from the channel activation and TFEB nuclear translocation and continues with the increased protein expression of the lysosomal channel. This is also proved by the increased expression of the motor neuron marker SMI 32 which was preserved in F1-treated transgenic mice together with a reduction of gliosis and microgliosis. Furthermore, while PI(3,5)P_2 immunosignal was highly reduced in the spinal cord of symptomatic

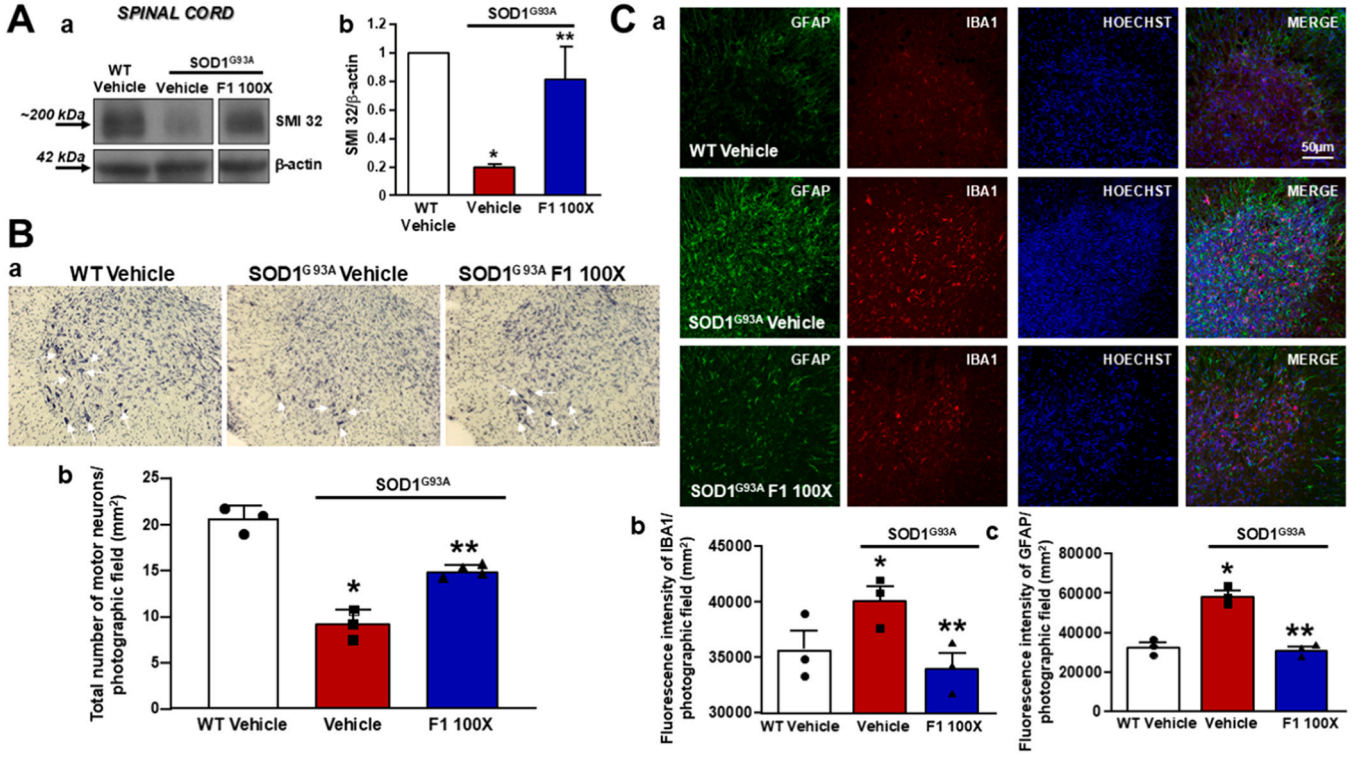

Fig. 8. SANP-PI(3,5)P_2 (F1) treatment from the presymptomatic stage reduces astrogliosis and microgliosis in spinal cords of symptomatic SOD1^{G93A} mice at 4,5 months, (A) Representative Western blotting (a) and quantification (b) of SMI 32 expression in the spinal cords of WT and symptomatic SOD1^{G93A} mice injected with physiological solution (WT Vehicle; SOD1^{G93A} Vehicle, respectively) and SOD1^{G93A} mice injected with F1 (100X). The latter group was treated with the preparation once a week for 6 weeks from the presymptomatic stage. Data are presented as means ± SEM. *p<0.05 WT; **p<0.05 vs SOD1^{G93A}. (B) Representative images (a) of spinal cord sections stained with gallocyanin representing different regions of the lumbar spinal cord L1 to L6. Quantification (b) of MNs in 3 sections selected at equally spaced intervals spanning L1–6 under 20× magnification (n = 3 mice for each experimental group). Data are presented as means ± SEM. *p<0.05 vs WT; **p<0.05 vs SOD1^{G93A}. (C) Confocal images of immunofluorescence for GFAP (green), Iba1 (red) and Hoechst (blue) (a) in the thoracolumbar spinal cords of WT and SOD1^{G93A} mice injected with physiological solution (WT Vehicle; SOD1^{G93A} Vehicle, respectively) and SOD1^{G93A} mice injected with F1 (100X). The histograms in (b) and (c) represent the quantification (mean ± SD) of fluorescence intensity (as arbitrary units) for each immunosignal in at least three different sections for each experimental group. *p<0.05 vs WT; **p<0.05 vs SOD1^{G93A}. Scale bar: 50 μm.

SOD1^{G93A} animals, it was significantly restored in transgenic mice injected with this new formulation as a readout of lysosomal function restoration.

That TRPML1 may be considered a transferable pharmacological target in ALS originated from the evidence of a significant reduced expression level of the channel in human medulla oblongata *post-mortem* tissues from ALS patients. This is mirrored by symptomatic ALS mice in which TRPML1 protein expression was reduced in brainstem and spinal cord. Of note, mice treatment with the proposed formulation of its endogenous ligand restored TRPML1 expression in brainstem of mice thereby suggesting the possibility to induce a protective loop by peculiar lysosomal channel stimulation. Moreover, this restorative mechanism didn't occur in spinal cord of ALS mice, despite the recovery of motor functions. In this respect, in support of the present data, it has been proposed that brainstem is considered as the brain area playing a central role in locomotor control [84]. However, the integrated function of cortex, brainstem, and spinal cord networks in the control of locomotor function remains an unresolved physiologic issue [84].

Another important issue deserving attention is the question of drug delivery to the central nervous system during a neurodegenerative process. Originally SANPs were designed to deliver bisphosphonates such as zoledronic acid to the brain for the treatment of glioblastoma [28,29]; more recently, they have been successfully proposed for brain delivery of miRNA [30] or siRNA [31] as well as for reactive oxygen species scavenging in ischemia-mimicking conditions [85]. In fact, among the advantages offered by lipid SANP formulations, one of the most important is the ability to deliver drugs to the brain, as previously demonstrated by us [28–31]. However, the penetration of the blood-brain barrier during ALS remains an issue not sufficiently addressed. Therefore, in the present study, we decided to use an *icv* administration route pointing out that much more effort should be done by experts to characterize the present formulation not only in ALS.

Collectively, the present data showed that PI(3,5)P_2 in lipid self-assembling nanoparticles, stabilizing TRPML1 function, may exert neuroprotective effects in ALS preclinical models through the restoration of correct autophagy thus identifying this lysosomal channel as a putative target in ALS therapy. Moreover, to definitively prove the pharmacological efficacy of the present approach, optimization of this formulation's bioavailability as well as more preclinical and/or clinical data should be pursued and collected prospectively in larger animal groups or through clinical trials.

CRediT authorship contribution statement

Giuseppe De Rosa: Supervision, Data curation, Conceptualization. **Anna Pannaccione:** Methodology, Data curation. **Valeria Nele:** Methodology, Investigation, Data curation. **Agnese Secondo:** Writing – review & editing, Writing – original draft, Resources, Data curation, Conceptualization. **Valentina Tedeschi:** Methodology, Data curation, Conceptualization. **Chiara Cassiano:** Investigation, Data curation. **Maria Josè Sisalli:** Investigation, Data curation. **Lorella Maria Teresa Canzoniero:** Writing – original draft. **Giuseppe Pignataro:** Methodology. **Valeria Valsecchi:** Methodology, Data curation. **Laura Zuccaro:** Methodology, Investigation, Data curation. **Serenella Anzilotti:**

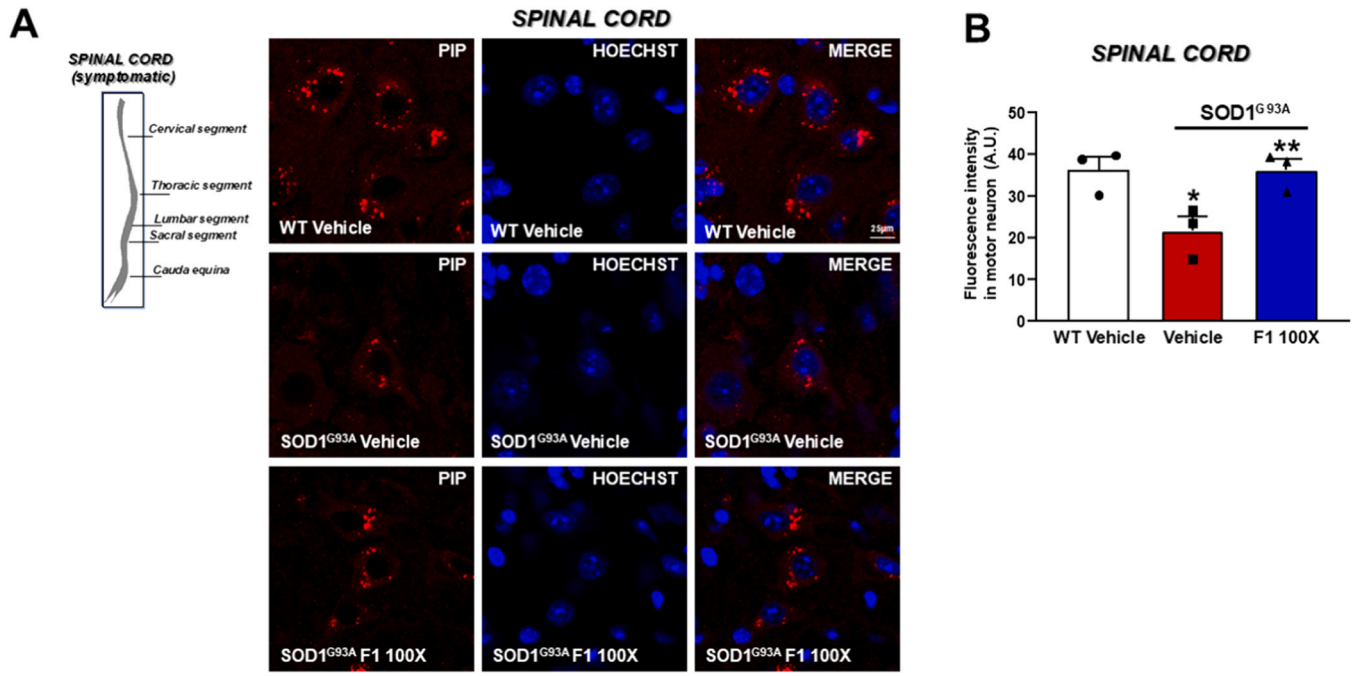

Fig. 9. F1 treatment from the presymptomatic stage restores endogenous level of PI(3,5)P_2 (PIP) in the spinal cords of symptomatic SOD1^{G93A} mice at motor neuronal level, (A) Immunofluorescence analysis of intracellular PI(3,5)P_2 (PIP) from WT mice injected with vehicle, and symptomatic SOD1^{G93A} mice injected with vehicle or F1 at 100X (PIP labelling in red, nuclei labelled with Hoechst dye in blue). F1 injected animals were treated in the presymptomatic stage **(B)** Quantification of PIP fluorescence intensity in neurons as arbitrary units (A.U.). Data are expressed as mean ± SEM (n = 3 for each group). *$p < 0.05$ vs WT Vehicle; **$p < 0.05$ vs SOD1^{G93A} Vehicle. Differences were analyzed by one-way ANOVA followed by Tukey's post-hoc analysis.

Methodology, Data curation. **Nunzia De Iesu:** Methodology. **Antonio Vinciguerra:** Methodology, Data curation.

Declaration of Competing Interest

The authors declare that they have no known competing financial interests or personal relationships that could have appeared to influence the work reported in this paper.

Appendix A. Supporting information

Supplementary data associated with this article can be found in the online version at doi:10.1016/j.phrs.2024.107491.

Data Availability

Data will be made available on request.

References

[1] A. Chiò, G. Logroscino, B.J. Traynor, J. Collins, J.C. Simeone, L.A. Goldstein, L. A. White, Global epidemiology of amyotrophic lateral sclerosis: a systematic review of the published literature, Neuroepidemiology 41 (2013) 118–130, https://doi.org/10.1159/000351153.

[2] J.P. Taylor, R.H. Brown, Jr, D.W. Cleveland, Decoding ALS: from genes to mechanism, Nature 539 (2016) 197–206, https://doi.org/10.1038/nature20413.

[3] O.M. Peters, M. Ghasemi, R.H. Brown Jr., Emerging mechanisms of molecular pathology in ALS, J. Clin. Invest 125 (2015) 1767–1779, https://doi.org/10.1172/JCI71601.

[4] M. Neumann, D.M. Sampathu, L.K. Kwong, A.C. Truax, M.C. Micsenyi, T.T. Chou, J. Bruce, T. Schuck, M. Grossman, C.M. Clark, L.F. McCluskey, B.L. Miller, E. Masliah, I.R. Mackenzie, H. Feldman, W. Feiden, H.A. Kretzschmar, J. Q. Trojanowski, V.M. Lee, Ubiquitinated TDP-43 in frontotemporal lobar degeneration and amyotrophic lateral sclerosis, Science 314 (2006) 130–133, https://doi.org/10.1126/science.1134108.

[5] D.B. Medinas, P. Rozas, F. Martínez Traub, U. Woehlbier, R.H. Brown, D.A. Bosco, C. Hetz, Endoplasmic reticulum stress leads to accumulation of wild-type SOD1 aggregates associated with sporadic amyotrophic lateral sclerosis, Proc. Natl. Acad. Sci. USA 115 (2018) 8209–8214, https://doi.org/10.1073/pnas.1801109115.

[6] D.A. Bosco, G. Morfini, N.M. Karabacak, Y. Song, F. Gros-Louis, P. Pasinelli, H. Goolsby, B.A. Fontaine, N. Lemay, D. McKenna-Yasek, M.P. Frosch, J.N. Agar, J. P. Julien, S.T. Brady, R.H. Brown Jr., Wild-type and mutant SOD1 share an aberrant conformation and a common pathogenic pathway in ALS, Nat. Neurosci. 13 (2010) 1396–1403, https://doi.org/10.1038/nn.2660.

[7] V. Tedeschi, T. Petrozziello, A. Secondo, Ca^{2+} dysregulation in the pathogenesis of amyotrophic lateral sclerosis, Int Rev. Cell Mol. Biol. 363 (2021) 21–47, https://doi.org/10.1016/bs.ircmb.2021.02.014.

[8] G. Le Masson, S. Przedborski, L.F. Abbott, A computational model of motor neuron degeneration, Neuron 83 (2014) 975–988, https://doi.org/10.1016/j.neuron.2014.07.001.

[9] C.J. Ferguson, G.M. Lenk, M.H. Meisler, PtdIns(3,5)P2 and autophagy in mouse models of neurodegeneration, Autophagy 6 (2010) 170–171, https://doi.org/10.4161/auto.6.1.10626.

[10] P.-W. Ko, Y.-S. Min, J.-S. Park, Likely pathogenic FIG4 related amyotrophic lateral sclerosis patient who correlated with clinical, imaging and neuropsychological studies, Ann. Clin. Neurophysiol. 22 (2020) 33–36, https://doi.org/10.14253/acn.2020.22.1.33.

[11] A. Osmanovic, I. Rangnau, A. Kosfeld, S. Abdulla, C. Janssen, B. Auber, P. Raab, M. Preller, S. Petri, R.G. Weber, FIG4 variants in central European patients with amyotrophic lateral sclerosis: a whole-exome and targeted sequencing study, Eur. J. Hum. Genet 25 (2017) 324–331, https://doi.org/10.1038/ejhg.2016.186.

[12] V. Tedeschi, S. Sapienza, R. Ciancio, L.M.T. Canzoniero, A. Pannaccione, A. Secondo, Lysosomal channels as new molecular targets in the pharmacological therapy of neurodegenerative diseases via autophagy regulation, Curr. Neuropharmacol. (2024), https://doi.org/10.2174/1570159X22666240517101846.

[13] D.L. Medina, S. Di Paola, I. Peluso, A. Armani, D. De Stefani, R. Venditti, S. Montefusco, A. Scotto-Rosato, C. Prezioso, A. Forrester, C. Settembre, W. Wang, Q. Gao, H. Xu, M. Sandri, R. Rizzuto, M.A. De Matteis, A. Ballabio, Lysosomal calcium signalling regulates autophagy through calcineurin and TFEB, Nat. Cell Biol. 17 (2015) 288–299, https://doi.org/10.1038/ncb3114.

[14] M. Sardiello, M. Palmieri, A. di Ronza, D.L. Medina, M. Valenza, V.A. Gennarino, C. Di Malta, F. Donaudy, V. Embrione, R.S. Polishchuk, S. Banfi, G. Parenti, E. Cattaneo, A. Ballabio, A gene network regulating lysosomal biogenesis and function, Science 325 (2009) 473–477, https://doi.org/10.1126/science.1174447.

[15] W. Song, F. Wang, M. Savini, A. Ake, A. di Ronza, M. Sardiello, L. Segatori, TFEB regulates lysosomal proteostasis, Hum. Mol. Genet. 22 (2013) 1994–2009, https://doi.org/10.1093/hmg/ddt052.

[16] V. Tedeschi, T. Petrozziello, M.J. Sisalli, F. Boscia, L.M.T. Canzoniero, A. Secondo, The activation of Mucolipin TRP channel 1 (TRPML1) protects motor neurons from L-BMAA neurotoxicity by promoting autophagic clearance, Sci. Rep. 9 (2019) 10743, https://doi.org/10.1038/s41598-019-46708-5.

[17] J. Zou, B. Hu, S. Arpag, Q. Yan, A. Hamilton, Y.S. Zeng, C.G. Vanoye, J. Li, Reactivation of lysosomal Ca^{2+} efflux rescues abnormal lysosomal storage in FIG4-

deficient cells, J. Neurosci. 35 (2015) 6801–6812, https://doi.org/10.1523/JNEUROSCI.4442-14.2015.
[18] J.K. Lee, J.H. Shin, J.E. Lee, E.J. Choi, Role of autophagy in the pathogenesis of amyotrophic lateral sclerosis, Biochim Biophys. Acta 1852 (2015) 2517–2524, https://doi.org/10.1016/j.bbadis.2015.08.005.
[19] J.J. Yerbury, N.E. Farrawell, L. McAlary, Proteome homeostasis dysfunction: a unifying principle in ALS pathogenesis, Trends Neurosci. 43 (2020) 274–284, https://doi.org/10.1016/j.tins.2020.03.002.
[20] B. Ravikumar, C. Vacher, Z. Berger, J.E. Davies, S. Luo, L.G. Oroz, F. Scaravilli, D. F. Easton, R. Duden, C.J. O'Kane, D.C. Rubinsztein, Inhibition of mTOR induces autophagy and reduces toxicity of polyglutamine expansions in fly and mouse models of Huntington disease, Nat. Genet 36 (2004) 585–595, https://doi.org/10.1038/ng1362.
[21] E. Bachar-Wikstrom, J.D. Wikstrom, Y. Ariav, B. Tirosh, N. Kaiser, E. Cerasi, G. Leibowitz, Stimulation of autophagy improves endoplasmic reticulum stress-induced diabetes, Diabetes 62 (2013) 1227–1237, https://doi.org/10.2337/db12-1474.
[22] I.F. Wang, B.S. Guo, Y.C. Liu, C.C. Wu, C.H. Yang, K.J. Tsai, C.K. Shen, Autophagy activators rescue and alleviate pathogenesis of a mouse model with proteinopathies of the TAR DNA-binding protein 43, Proc. Natl. Acad. Sci. USA 109 (2012) 15024–15029, https://doi.org/10.1073/pnas.1206362109.
[23] J. Mandrioli, R. D'Amico, E. Zucchi, A. Gessani, N. Fini, A. Fasano, C. Caponnetto, A. Chiò, E. Dalla Bella, C. Lunetta, L. Mazzini, K. Marinou, G. Sorarù, S. de Biasi, D. Lo Tartaro, M. Pinti, A.R.A.P.-A.L.S. investigators group Cossarizza, Rapamycin treatment for amyotrophic lateral sclerosis: protocol for a phase II randomized, double-blind, placebo-controlled, multicenter, clinical trial (RAP-ALS trial), Med. (Baltim.) 97 (2018) e11119, https://doi.org/10.1097/MD.0000000000011119.
[24] D.K.H. Nguyen, R. Thombre, J. Wang, Autophagy as a common pathway in amyotrophic lateral sclerosis, Neurosci. Lett. 697 (2019) 34–48, https://doi.org/10.1016/j.neulet.2018.04.006.
[25] Q.J. Wang, Y. Ding, D.S. Kohtz, N. Mizushima, I.M. Cristea, M.P. Rout, B.T. Chait, Y. Zhong, N. Heintz, Z. Yue, Induction of autophagy in axonal dystrophy and degeneration, J. Neurosci. 26 (2006) 8057–8068, https://doi.org/10.1523/JNEUROSCI.2261-06.2006.
[26] N. Gan, Y. Han, W. Zeng, Y. Wang, J. Xue, Y. Jiang, Structural mechanism of allosteric activation of TRPML1 by PI(3,5)P_2 and rapamycin, Proc. Natl. Acad. Sci. USA 119 (2022) e2120404119, https://doi.org/10.1073/pnas.2120404119.
[27] V. Nele, V. Campani, S. Alia Moosavian, G. De Rosa, Lipid nanoparticles for RNA delivery: self-assembling vs driven-assembling strategies, Adv. Drug Deliv. Rev. 208 (2024) 115291, https://doi.org/10.1016/j.addr.2024.115291.
[28] M. Porru, S. Zappavigna, G. Salzano, A. Luce, A. Stoppacciaro, M.L. Balestrieri, S. Artuso, S. Lusa, G. De Rosa, C. Leonetti, M. Caraglia, Medical treatment of orthotopic glioblastoma with transferrin-conjugated nanoparticles encapsulating zoledronic acid, Oncotarget 5 (2014) 10446–10459, https://doi.org/10.18632/oncotarget.2182.
[29] M. Abate, L. Scotti, V. Nele, M. Caraglia, M. Biondi, G. De Rosa, C. Leonetti, V. Campani, S. Zappavigna, M. Porru, Hybrid self-assembling nanoparticles encapsulating zoledronic acid: a strategy for fostering their clinical use, Int J. Mol. Sci. 23 (2022) 5138, https://doi.org/10.3390/ijms23095138.
[30] V. Campani, S. Zappavigna, L. Scotti, M. Abate, M. Porru, C. Leonetti, M. Caraglia, G. De Rosa, Hybrid lipid self-assembling nanoparticles for brain delivery of microRNA, Int J. Pharm. 588 (2020) 119693, https://doi.org/10.1016/j.ijpharm.2020.119693.
[31] R. Delle Donne, R. Iannucci, L. Rinaldi, L. Roberto, M.A. Oliva, E. Senatore, D. Borzacchiello, L. Lignitto, G. Giurato, F. Rizzo, A. Sellitto, F. Chiuso, S. Castaldo, G. Scala, V. Campani, V. Nele, G. De Rosa, C. D'Ambrosio, C. Garbi, A. Scaloni, A. Weisz, C. Ambrosino, A. Arcella, A. Feliciello, Targeted inhibition of ubiquitin signaling reverses metabolic reprogramming and suppresses glioblastoma growth, Commun. Biol. 5 (2022) 780, https://doi.org/10.1038/s42003-022-03639-8.
[32] T.J. Montine, C.H. Phelps, T.G. Beach, E.H. Bigio, N.J. Cairns, D.W. Dickson, C. Duyckaerts, M.P. Frosch, E. Masliah, S.S. Mirra, P.T. Nelson, J.A. Schneider, D. R. Thal, J.Q. Trojanowski, H.V. Vinters, B.T. Hyman, National Institute on Aging; Alzheimer's Association. National Institute on Aging-Alzheimer's Association guidelines for the neuropathologic assessment of Alzheimer's disease: a practical approach, Acta Neuropathol. 123 (2012) 1–11, https://doi.org/10.1007/s00401-011-0910-3.
[33] D.R. Thal, U. Rüb, M. Orantes, H. Braak, Phases of A beta-deposition in the human brain and its relevance for the development of AD, Neurology 58 (2002) 1791–1800, https://doi.org/10.1212/wnl.58.12.1791.
[34] H. Braak, E. Braak, Neuropathological stageing of Alzheimer-related changes, Acta Neuropathol. 82 (1991) 239–359, https://doi.org/10.1007/BF00308809.
[35] H. Braak, I. Alafuzoff, T. Arzberger, H. Kretzschmar, K. Del Tredici, Staging of Alzheimer disease-associated neurofibrillary pathology using paraffin sections and immunocytochemistry, Acta Neuropathol. 112 (2006) 389–404, https://doi.org/10.1007/s00401-006-0127-z.
[36] S.S. Mirra, A. Heyman, D. McKeel, S.M. Sumi, B.J. Crain, L.M. Brownlee, F.S. Vogel, J.P. Hughes, van, G. Belle, L. Berg, The Consortium to Establish a Registry for Alzheimer's Disease (CERAD). Part II. Standardization of the neuropathologic assessment of Alzheimer's disease, Neurology 41 (1991) 479–486, https://doi.org/10.1212/wnl.41.4.479.
[37] T. Petrozziello, A. Secondo, V. Tedeschi, A. Esposito, M. Sisalli, A. Scorziello, G. Di Renzo, L. Annunziato, ApoSOD1 lacking dismutase activity neuroprotects motor neurons exposed to beta-methylamino-L-alanine through the Ca^{2+}/Akt/ERK1/2 prosurvival pathway, Cell Death Differ. 24 (2017) 511–522, https://doi.org/10.1038/cdd.2016.154.
[38] R. Khosla, H. Bhagat, P. Lal, A. Anand, ALS plasma reduces the viability of NSC34 cells via altering mRNA expression of VEGF: a short report, Heliyon 9 (2023) e18287, https://doi.org/10.1016/j.heliyon.2023.e18287.
[39] R. Stifanese, M. Averna, R. De Tullio, M. Pedrazzi, F. Beccaria, F. Salamino, M. Milanese, G. Bonanno, S. Pontremoli, E. Melloni, Adaptive modifications in the calpain/calpastatin system in brain cells after persistent alteration in Ca^{2+} homeostasis, J. Biol. Chem. 285 (2010) 631–643, https://doi.org/10.1074/jbc.M109.031674.
[40] M.E. Gurney, The use of transgenic mouse models of amyotrophic lateral sclerosis in preclinical drug studies, J. Neurol. Sci. 152 (1997) S67–S73, https://doi.org/10.1016/s0022-510x(97)00247-5.
[41] X. Ge, A. Cho, M.A. Ciol, C. Pettan-Brewer, J. Snyder, P. Rabinovitch, W. Ladiges, Grip strength is potentially an early indicator of age-related decline in mice, Pathobiol. Aging Age Relat. Dis. 6 (2016) 32981, https://doi.org/10.3402/pba.v6.32981.
[42] S. Apolloni, S. Amadio, P. Fabbrizio, G. Morello, A.G. Spampinato, E.C. Latagliata, I. Salvatori, D. Proietti, A. Ferri, L. Madaro, S. Puglisi-Allegra, S. Cavallaro, C. Volonté, Histaminergic transmission slows progression of amyotrophic lateral sclerosis, J. Cachex-.-. Sarcopenia Muscle 10 (2019) 872–893, https://doi.org/10.1002/jcsm.12422.
[43] S. Migliarini, S. Scaricamazza, C. Valle, A. Ferri, M. Pasqualetti, E. Ferraro, Microglia morphological changes in the motor cortex of hSOD1^{G93A} transgenic ALS mice, Brain Sci. 11 (2021) 807, https://doi.org/10.3390/brainsci11060807.
[44] X. Wang, X. Zhang, X.P. Dong, M. Samie, X. Li, X. Cheng, A. Goschka, D. Shen, Y. Zhou, J. Harlow, M.X. Zhu, D.E. Clapham, D. Ren, H. Xu, TPC proteins are phosphoinositide- activated sodium-selective ion channels in endosomes and lysosomes, Cell 151 (2012) 372–383, https://doi.org/10.1016/j.cell.2012.08.036.
[45] X.P. Dong, D. Shen, X. Wang, T. Dawson, X. Li, Q. Zhang, X. Cheng, Y. Zhang, L. S. Weisman, M. Delling, H. Xu, PI(3,5)P(2) controls membrane trafficking by direct activation of mucolipin Ca(2+) release channels in the endolysosome. Nat. Commun. 1 (2010) 38, https://doi.org/10.1038/ncomms1037.
[46] X.Z. Zhong, X.P. Dong, Lysosome electrophysiology, Methods Cell Biol. 126 (2015) 197–215, https://doi.org/10.1016/bs.mcb.2014.10.022.
[47] X. Zhang, W. Chen, Q. Gao, J. Yang, X. Yan, H. Zhao, L. Su, M. Yang, C. Gao, Y. Yao, K. Inoki, D. Li, R. Shao, S. Wang, N. Sahoo, F. Kudo, T. Eguchi, B. Ruan, H. Xu, Rapamycin directly activates lysosomal mucolipin TRP channels independent of mTOR, PLoS Biol. 17 (2019) e3000252, https://doi.org/10.1371/journal.pbio.3000252.
[48] G. Grynkiewicz, M. Poenie, R.Y. Tsien, A new generation of Ca^{2+} indicators with greatly improved fluorescence properties, J. Biol. Chem. 260 (1985) 3440–3450.
[49] J. Urbanczyk, O. Chernysh, M. Condrescu, J.P. Reeves, Sodium-calcium exchange does not require allosteric calcium activation at high cytosolic sodium concentrations, J. Physiol. 575 (2006) 693–705, https://doi.org/10.1113/jphysiol.2006.113910.
[50] A.M. Surin, R.R. Sharipov, I.A. Krasil'nikova, D.P. Boyarkin, O.Y. Lisina, L. R. Gorbacheva, A.V. Avetisyan, V.G. Pinelis, Disruption of functional activity of mitochondria during MTT assay of viability of cultured neurons, Biochem. (Mosc. 82 (2017) 737–749, https://doi.org/10.1134/S0006297917060104.
[51] A. Secondo, R.I. Staiano, A. Scorziello, R. Sirabella, F. Boscia, A. Adornetto, V. Valsecchi, P. Molinaro, L.M. Canzoniero, G. Di Renzo, L. Annunziato, BHK cells transfected with NCX3 are more resistant to hypoxia followed by reoxygenation than those transfected with NCX1 and NCX2: Possible relationship with mitochondrial membrane potential, Cell Calcium 42 (2007) 521–535, https://doi.org/10.1016/j.ceca.2007.01.006.
[52] S. Anzilotti, V. Valente, P. Brancaccio, C. Franco, A. Casamassa, G. Lombardi, A. Palazzi, A. Conte, S. Paladino, L.M.T. Canzoniero, L. Annunziato, G. M. Pierantoni, G. Pignataro, Chronic exposure to l-BMAA cyanotoxin induces cytoplasmic TDP-43 accumulation and glial activation, reproducing an amyotrophic lateral sclerosis-like phenotype in mice, Biomed. Pharm. 167 (2023) 115503, https://doi.org/10.1016/j.biopha.2023.115503.
[53] P. Brancaccio, S. Anzilotti, O. Cuomo, A. Vinciguerra, M. Campanile, A. Herchuelz, S. Amoroso, L. Annunziato, G. Pignataro, Preconditioning in hypoxic-ischemic neonate mice triggers Na^+-Ca^{2+} exchanger-dependent neurogenesis, Cell Death Discov. 8 (2022) 318, https://doi.org/10.1038/s41420-022-01089-z.
[54] A. Vinciguerra, P. Cepparulo, S. Anzilotti, O. Cuomo, V. Valsecchi, S. Amoroso, L. Annunziato, G. Pignataro, Remote postconditioning ameliorates stroke damage by preventing let-7a and miR-143 up-regulation, Theranostics 10 (2020) 12174–12188, https://doi.org/10.7150/thno.48135.
[55] L. Sanguigno, A. Casamassa, N. Funel, M. Minale, R. Riccio, S. Riccio, F. Boscia, P. Brancaccio, L.E. Pollina, S. Anzilotti, G. Di Renzo, O. Cuomo, Triticum vulgare extract exerts an anti-inflammatory action in two in vitro models of inflammation in microglial cells, PLoS One 13 (2018) e0197493, https://doi.org/10.1371/journal.pone.0197493.
[56] S. Anzilotti, V. Valsecchi, P. Brancaccio, N. Guida, G. Laudati, V. Tedeschi, T. Petrozziello, F. Frecentese, E. Magli, B. Hassler, O. Cuomo, L. Formisano, A. Secondo, L. Annunziato, G. Pignataro, Prolonged NCX activation prevents SOD1 accumulation, reduces neuroinflammation, ameliorates motor behavior and prolongs survival in a ALS mouse model, Neurobiol. Dis. 159 (2021) 105480, https://doi.org/10.1016/j.nbd.2021.105480.
[57] V. Tedeschi, A. Secondo, Emerging role of lysosomal calcium store as a hub of neuroprotection, Neural Regen. Res 17 (2022) 1259–1260, https://doi.org/10.4103/1673-5374.327340.
[58] H. Xu, D. Ren, Lysosomal physiology, Annu Rev. Physiol. 77 (2015) 57–80, https://doi.org/10.1146/annurev-physiol-021014-071649.
[59] C. Curcio-Morelli, F.A. Charles, M.C. Micsenyi, Y. Cao, B. Venugopal, M. F. Browning, K. Dobrenis, S.L. Cotman, S.U. Walkley, S.A. Slaugenhaupt,

Macroautophagy is defective in mucolipin-1-deficient mouse neurons, Neurobiol. Dis. 40 (2010) 370–377, https://doi.org/10.1016/j.nbd.2010.06.010.
[60] D.L. Medina, A. Ballabio, Lysosomal calcium regulates autophagy, Autophagy 11 (2015) 970–971, https://doi.org/10.1080/15548627.2015.1047130.
[61] F. Guo, X. Liu, H. Cai, W. Le, Autophagy in neurodegenerative diseases: pathogenesis and therapy, Brain Pathol. 28 (2018) 3–13, https://doi.org/10.1111/bpa.12545.
[62] A. Eisen, M. Weber, The motor cortex and amyotrophic lateral sclerosis, Muscle Nerve 24 (2001) 564–573, https://doi.org/10.1002/mus.1042.
[63] X.P. Dong, X. Cheng, E. Mills, M. Delling, F. Wang, T. Kurz, H. Xu, The type IV mucolipidosis-associated protein TRPML1 is an endolysosomal iron release channel, Nature 455 (2008) 992–996, https://doi.org/10.1038/nature07311.
[64] X. Zhang, X. Li, H. Xu, Phosphoinositide isoforms determine compartment-specific ion channel activity, Proc. Natl. Acad. Sci. USA 109 (2012) 11384–11389, https://doi.org/10.1073/pnas.1202194109.
[65] H.H. Bui, P.E. Sanders, D. Bodenmiller, M.S. Kuo, G.P. Donoho, A.S. Fischl, Direct analysis of PI(3,4,5)P_3 using liquid chromatography electrospray ionization tandem mass spectrometry, Anal. Biochem 547 (2018) 66–76, https://doi.org/10.1016/j.ab.2018.02.014.
[66] M. Saito, P.I. Hanson, P. Schlesinger, Luminal chloride-dependent activation of endosome calcium channels: patch clamp study of enlarged endosomes, J. Biol. Chem. 282 (2007) 27327–27333, https://doi.org/10.1074/jbc.M702557200.
[67] P.R. Pryor, F. Reimann, F.M. Gribble, J.P. Luzio, Mucolipin-1 is a lysosomal membrane protein required for intracellular lactosylceramide traffic, Traffic 7 (2006) 1388–1398, https://doi.org/10.1111/j.1600-0854.2006.00475.x.
[68] S. Vergarajauregui, R. Puertollano, Two di-leucine motifs regulate trafficking of mucolipin-1 to lysosomes, Traffic 7 (2006) 337–353, https://doi.org/10.1111/j.1600-0854.2006.00387.x.
[69] C. Settembre, R. Zoncu, D.L. Medina, F. Vetrini, S. Erdin, S. Erdin, T. Huynh, M. Ferron, G. Karsenty, M.C. Vellard, V. Facchinetti, D.M. Sabatini, A. Ballabio, A lysosome-to-nucleus signalling mechanism senses and regulates the lysosome via mTOR and TFEB, EMBO J. 31 (2012) 1095–1108, https://doi.org/10.1038/emboj.2012.32.
[70] B. Levine, G. Kroemer, Autophagy in the pathogenesis of disease, Cell 132 (2008) 27–42, https://doi.org/10.1016/j.cell.2007.12.018.
[71] P. Boya, G. Kroemer, Lysosomal membrane permeabilization in cell death, Oncogene 27 (2008) 6434–6451, https://doi.org/10.1038/onc.2008.310.
[72] Q. Chen, J. She, W. Zeng, J. Guo, H. Xu, X.C. Bai, Y. Jiang, Structure of mammalian endolysosomal TRPML1 channel in nanodiscs, Nature 550 (2017) 415–418, https://doi.org/10.1038/nature24035.
[73] M. Fine, P. Schmiege, X. Li, Structural basis for PtdInsP_2-mediated human TRPML1 regulation, Nat. Commun. 9 (2018) 4192, https://doi.org/10.1038/s41467-018-06493-7.
[74] T. Jiang, J.T. Yu, X.C. Zhu, M.S. Tan, H.F. Wang, L. Cao, Q.Q. Zhang, J.Q. Shi, L. Gao, H. Qin, Y.D. Zhang, L. Tan, Temsirolimus promotes autophagic clearance of amyloid-β and provides protective effects in cellular and animal models of Alzheimer's disease, Pharm. Res 81 (2014) 54–63, https://doi.org/10.1016/j.phrs.2014.02.008.
[75] T. Jiang, J.T. Yu, X.C. Zhu, Q.Q. Zhang, L. Cao, H.F. Wang, M.S. Tan, Q. Gao, H. Qin, Y.D. Zhang, L. Tan, Temsirolimus attenuates tauopathy in vitro and in vivo by targeting tau hyperphosphorylation and autophagic clearance, Neuropharmacology 85 (2014) 121–130, https://doi.org/10.1016/j.neuropharm.2014.05.032.
[76] M. Bae, N. Patel, H. Xu, M. Lee, K. Tominaga-Yamanaka, A. Nath, J. Geiger, M. Gorospe, M.P. Mattson, N.J. Haughey, Activation of TRPML1 clears intraneuronal Aβ in preclinical models of HIV infection, J. Neurosci. 34 (2014) 11485–11503, https://doi.org/10.1523/JNEUROSCI.0210-14.2014.
[77] L. Zhang, Y. Fang, X. Cheng, Y. Lian, H. Xu, Z. Zeng, H. Zhu, TRPML1 participates in the progression of Alzheimer's disease by regulating the PPARγ/AMPK/Mtor signalling pathway, Cell Physiol. Biochem 43 (2017) 2446–2456, https://doi.org/10.1159/000484449.
[78] A. Somogyi, E.D. Kirkham, E. Lloyd-Evans, J. Winston, N.D. Allen, J.J. Mackrill, K. E. Anderson, P.T. Hawkins, S.E. Gardiner, H. Waller-Evans, R. Sims, B. Boland, C. O'Neill, The synthetic TRPML1 agonist ML-SA1 rescues Alzheimer-related alterations of the endosomal-autophagic-lysosomal system, J. Cell Sci. 136 (2023) jcs259875, https://doi.org/10.1242/jcs.259875.
[79] X.J. Guan, Z.Q. Deng, J. Liu, C.F. Su, B.C. Tong, Z. Zhu, S.G. Sreenivasmurthy, Y. X. Kan, K.J. Lu, C.P. Chu, R.B. Pi, K.H. Cheung, A. Iyaswamy, J.X. Song, M. Li, Corynoxine promotes TFEB/TFE3-mediated autophagy and alleviates Aβ pathology in Alzheimer's disease models, Acta Pharm. Sin. 45 (2024) 900–913, https://doi.org/10.1038/s41401-023-01197-1.
[80] M.R. Pollmanns, J. Beer, I. Rosignol, N. Rodriguez-Muela, B.H. Falkenburger, E. Dinter, Activated endolysosomal cation channel TRPML1 facilitates maturation of α-synuclein-containing autophagosomes, Front Cell Neurosci. 16 (2022) 861202, https://doi.org/10.3389/fncel.2022.861202.
[81] L.K. Wu, S. Agarwal, C.H. Kuo, Y.L. Kung, C.H. Day, P.Y. Lin, S.Z. Lin, D.J. Hsieh, C. Y. Huang, C.Y. Chiang, Artemisia Leaf Extract protects against neuron toxicity by TRPML1 activation and promoting autophagy/mitophagy clearance in both in vitro and in vivo models of MPP^+/MPTP-induced Parkinson's disease, Phytomedicine 104 (2022) 154250, https://doi.org/10.1016/j.phymed.2022.154250.
[82] Y. Date, Y. Sasazawa, M. Kitagawa, K. Gejima, A. Suzuki, H. Saya, Y. Kida, M. Imoto, E. Itakura, N. Hattori, S. Saiki, Novel autophagy inducers by accelerating lysosomal clustering against Parkinson's disease, Elife 13 (2024) e98649, https://doi.org/10.7554/eLife.98649.
[83] M. Palmieri, S. Impey, H. Kang, A. di Ronza, C. Pelz, M. Sardiello, A. Ballabio, Characterization of the CLEAR network reveals an integrated control of cellular clearance pathways, Hum. Mol. Genet 20 (2011) 3852–3866, https://doi.org/10.1093/hmg/ddr306.
[84] R. Leiras, J.M. Cregg, O. Kiehn, Brainstem circuits for locomotion, Annu Rev. Neurosci. 45 (2022) 63–85, https://doi.org/10.1146/annurev-neuro-082321-025137.
[85] V. Nele, V. Tedeschi, V. Campani, R. Ciancio, A. Angelillo, S.F. Graziano, G. De Rosa, A. Secondo, Cerium-doped self-assembling nanoparticles as a novel anti-oxidant delivery system preserving mitochondrial function in cortical neurons exposed to Ischemia-like conditions, Antioxidants 12 (2023) 358, https://doi.org/10.3390/antiox12020358.